Evolution and Reversibility of Host/Guest Interactions with Temperature Changes in a Methyl Red@Palygorskite Polyfunctional Hybrid Nanocomposite

(Article begins on next page)

25 April 2024

Evolution and reversibility of host/guest interactions with temperature changes in a methyl red@palygorskite polyfunctional hybrid nanocomposite

Roberto Giustetto,*[1] Jenny G. Vitillo,[2,3] Ingrid Corazzari,[3] Francesco Turci[3]

[1]Department of Earth Sciences and NIS, Nanostructured Interfaces and Surfaces Centre, Università degli Studi di Torino, Via Valperga Caluso 35, 10125 Torino (Italy)

[2]Department of Science and High Technology, University of Insubria, and INSTM Unit, Via Lucini 3, 22100 Como (Italy)

[3]Department of Chemistry, "G. Scansetti" Interdepartmental Centre for Studies on Asbestos and other Toxic particulates and NIS, Nanostructured Interfaces and Surfaces Centre, Università degli Studi di Torino, via Pietro Giuria 7, 10125 Torino (Italy).

*Corresponding author e-mail: roberto.giustetto@unito.it

Evolution and reversibility of host/guest interactions with temperature changes in a methyl red@palygorskite polyfunctional hybrid nanocomposite

Abstract

Palygorskite is a microporous clay mineral with several important applications, including use as dye nano-scaffold, due to its ability to incorporate apt guest molecules and form exceptionally stable composites. Such a property covers widespread fields of interest, from pottery pigments to light harvesting. In all these applications, the stability of these composites at progressively increasing temperatures is an important parameter to determine their condition of usage. This work investigates the nature and strength of the stabilizing host/guest interactions at the basis of the exceptional stability of the methyl red@palygorskite composite system, which undergo a dynamic but reversible evolution depending on the level of heating. A multi-technique analytical protocol involving synchrotron X-ray powder diffraction (S-XRPD) and thermogravimetric analysis (TGA) coupled with infrared spectroscopy (FT-IR) and gas chromatography (GC-MS) was followed, which allowed to sharply identify the species evolved during heating. Moderate temperatures (140°-300°C) cause stabilization of H-bonds between the structural H_2O and the carboxyl group of the dye, whereas higher ones (> 300°C) trigger formation of direct COOH/octahedral Mg bonds favoured by dehydration. Cooling below 300°C implies gradual reversibility of the observed trend due to rehydration from environmental moisture; additional heating (> 400°C), conversely, causes methyl red decomposition, fragmentation and further expulsion from the host tunnels (~ 500°C). The encapsulated dye in zwitterionic, trans and/or protonated form affects the hosting system properties, preventing structural folding and strongly modifying the mechanism of water release for both structural and zeolitic H_2O. Experimental results were interpreted also with the help of structural models obtained by molecular mechanics simulations, offering atomistic insights on the mechanisms at the basis of the observed phenomena.

1. Introduction

The importance of inclusion compounds is fundamental in nowadays scientific research, due to their versatile applications in Materials Science. The encapsulation of guest molecules or nanoclusters within inorganic frameworks can lead to the synthesis of innovative materials with peculiar properties, apt to be used for optical carriage, energy transfer, polymer reinforcement, control release, drug delivery, gas storage and catalysis.[1] Although zeolites and other feldspatoids are fit hosting matrices,[2] other microporous minerals can be used as well in which the guest is adsorbed on the crystal surface[3] or juxtaposed in structure permeating cavities.[4] Palygorskite (PALY hereafter) is a microporous clay phyllosilicate mineral, with ideal formula $(Mg,Al)_4Si_8O_{20}(OH)_2(H_2O)_4 \cdot 4H_2O$ and Mg/Al ratio ≤ 1[5,6] (Figure 1.a), occurring in nature as a variable mixture of two polymorphs – monoclinic (space group: *C2/m*) and orthorhombic (*Pbmn*).[7-11] In its structure, along the *x* crystallographic axis a discontinuous octahedral sheet (O) alternates with a waving tetrahedral one (T), whose apical oxygens periodically invert their orientation bonding to the upper or lower O strip.[12] Such a chessboard-like arrangement of interconnected TOT ribbons[13] causes the framework to be permeated by *z*-elongated tunnels (maximum width: 6.4 Å) filled by weakly bound (zeolitic) H_2O. Tightly bound (structural) water (indicated in specialized literature as OH_2)[14] completes the coordination of Mg ions located in the *M3* sites on the borders of the O ribbons, whereas Al preferentially occupies the internal *M2* sites.[15] The monodimensionality of these pores and their small maximum effective width,

coupled with the high cation density, make PALY a suitable material for a number of sorption-related applications, including lubricant, sorbent, excipient in drugs,[16] entrapment of heavy metal ions,[17] purification of wastewaters,[18] and physi-/chemisorption of drugs and dyes (i.e. isoniazid, methylene blue and crystal violet).[19] This clay mineral is in fact the host inorganic component of the indigo-based pigment Maya Blue,[20-22] aptly defined in literature as a complex polyfunctional organic-inorganic hybrid material[23-25] well known for its astounding resistance to chemical agents and light exposure.[26-29]

Although other authors tried to simulate the Maya Blue features by encapsulating indigo in different microporous matrices,[30-32] an even more attractive perspective can be pursued by achieving incorporation of other dyes of appropriate dimensions and reactivity in the PALY tunnels, thus exploiting this clay sorption properties to produce innovative and differently coloured hybrid materials. In particular, methyl red (Fig. 1.b) has been reported to be able to feasibly encapsulate within the PALY tunnels, thus forming a nanocomposite which owns the very same chemical and photo-stability of its renowned predecessor but a reddish/purple colour instead. For such a reason, the term "*Maya Red*" pigment was tentatively proposed as a suitable name for this hybrid material.[33,34] According to some authors, one of the essential conditions to be accomplished by original "Mayan" materials is the oxidation/reduction cycle undergone by some of the guest molecules during preparation of the pigment. This particular mechanism (redox tuning) causes different topological isomers to be fixated to the palygorskite framework in genuine Maya Blue (i.e. indigo, dehydroindigo and isatin), each contributing to this polyfunctional hybrid colour.[23-25,35,36] However, as no general agreement yet exists in the scientific literature about what materials should be properly termed as "Mayan" or else (except for genuine, historic Mayan pigments themselves), the name "*Maya Red*" was preferably left out in order to avoid any misunderstanding. Consistently with the nomenclature adopted in literature for other analogous materials,[30,36] this composite will therefore be termed methyl red@palygorskite (or METHYLRED@PALY) hereafter.
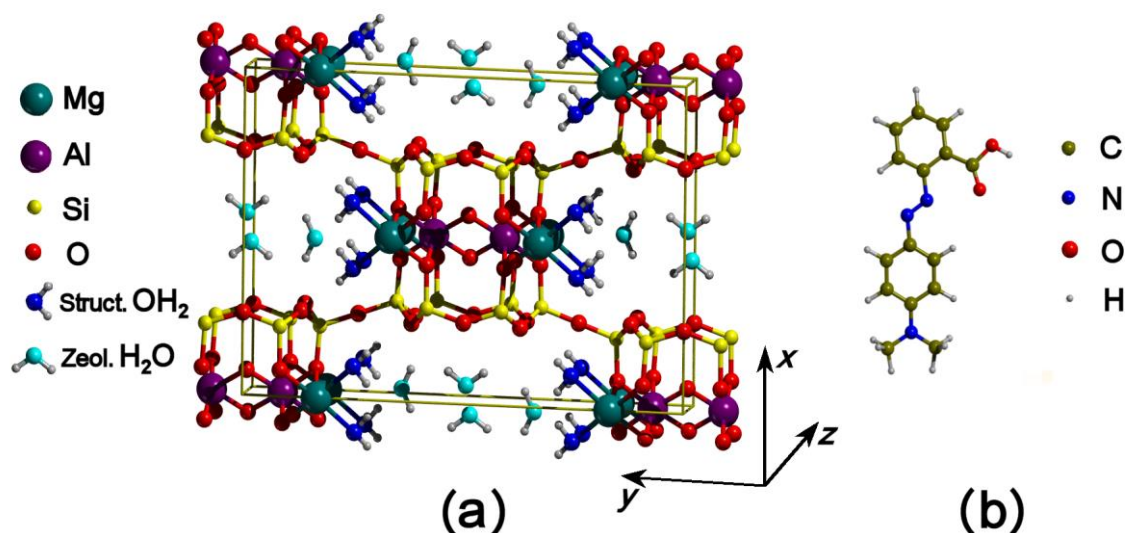
Figure 1. The structure of monoclinic palygorskite;[9] unit cell is evidenced by continuous lines (a). Trans conformer of the Acid red 2 (methyl red) dye molecule (b).

This paper is aimed to investigate the evolution, both in nature and strength, of the various kinds of host/guest interactions established in the tunnels of METHYLRED@PALY at progressively increasing temperatures, responsible for the extraordinary stability of this hybrid composite. Similarly to Maya Blue,[37,38] in fact, different kinds of host/guest interactions are possibly expected to play a fundamental role in stabilizing the relationships between the clay and the dye. An innovative approach for this kind of systems was used, involving synchrotron generated X-ray powder diffractograms (S-XRPD) and thermogravimetric analysis (TGA) coupled with time-resolved FTIR and GC-MS screening of the evolved gas, so to gain insight of the molecular surroundings of methyl red in the clay tunnels and understand the interactions at the basis of METHYLRED@PALY exceptional stability. Such a procedure allowed to accurately study the chemical environment of the different adsorption sites available for methyl red in the PALY framework at variable temperatures and the tendency, for these sites, to mutually interchange while heating or cooling. This phenomenon is strictly related to the dehydration mechanism (release of structural and zeolitic water) of the hybrid composite, which was carefully monitored throughout a wide temperature range until degradation and release of the clay-incorporated

methyl red occurred. Molecular mechanics calculations were performed both to obtain structural models of the dye/clay composite and calculate the binding energies of structural and zeolitic water. This possibly facilitates the interpretation of the experimental results and the comprehension of the multi-step water release observed in the dye/clay system, proposed here to be a capping-hopping process.

2. Experimental

2.1 Synthesis

Natural PALY coming from Chiapas (Mexico) was hand-ground and dispersed into deionised water, thus isolating the thinner suspended fraction from the heavier quartz (SiO_2) and calcite ($CaCO_3$) impurities.[39] Powders were then soaked in diluted HCl (20%) for 1 min to eliminate residual fine-grained calcite and repeatedly washed in deionised H_2O. XRPD proved PALY to be the only detectable phase, its structure unaffected by the acid treatment. Solid acid red 2-(methyl red) powder [$4-(CH_3)_2NC_6H_4N:NC_6H_4\cdot2-COOH$] was provided by Carlo Erba (C.I. 13020). The synthesis procedure of this hybrid nanocomposite formed by adding methyl red (2 wt%) to PALY was modeled upon the laboratory preparation of Maya Blue from pure precursors.[27,28,40,41] Purified PALY was crushed, mixed and ground with methyl red powder (2 wt%, consistently with the average indigo content in Maya Blue)[42,43] adding few ethanol drops. Such an orange mixture, which turned to brilliant red after few minutes, was dispersed in a Petri dish with diluted HCl (20%), heated at 20°C/h up to 140°C, and left at this temperature for 20 h. The obtained red-purplish adduct was Soxhlet-extracted in ethanol to remove the dye excess and then dried in air. The resulting bright purple-violet powder (METHYLRED@PALY) was recovered and used as such in all experiments.

2.2 Methods

Synchrotron XRPD data were collected at the European Synchrotron Radiation Facility (ESRF) in Grenoble, France, on the ID31 beam line using a wavelength of $\lambda = 0.7998$ Å in Debye-Scherrer geometry. Hand ground samples were loaded into 0.5 mm diameter quartz-glass capillaries in order to reduce preferred orientation effects. Diffracted beams were collected by an array of nine detectors supplied with a monochromator to eliminate fluorescence effects. Raw data were reduced by standard ID31 procedure for each detector and binned together. Data were processed using the GSAS-EXPGUI software.[44] Molecular mechanics simulations, in the form of classic atomistic lattice energy minimizations, were performed with the Discover 2009.1 program as implemented in the Materials Studio 5.0 package of Accelrys Inc..[45] The augmented version of the consistent-valence forcefield[46] (CVFF-AUG) was adopted because of its good performances in analogous studies.[42,47-49] Periodic boundary conditions and net formal charges for all ions were adopted. Charges for methyl red (in trans- and protonated form) were obtained by optimizing the structure at the CAM-B3LYP/TZV2p level, by means of the *Gaussian09* program,[51] as Mulliken charges. The trans- and protonated methyl red electrostatic potential (ESP) maps were evaluated at the same level of approximation. Although these ESP maps cannot exhaustively describe the considered system and, consequently, the details of the feasible clay/dye interactions due to missing of both the polarization and electronic effects, they are known to be a very useful tool in order to understand and explain the nature of the possible intermolecular interactions.[52,53] Electrostatic interactions were handled using the Ewald summation technique (accuracy set to $2\mathrm{x}10^{-4}$ kJ·mol^{-1}). P_1 symmetry was used in all the calculations. Each optimized structure was allowed to relax at constant pressure ($P = 0$) by means of the BFGS method (convergence criteria set to 4.1 mJ mol^{-1} Å^{-1}). Computed binding energy (BE) was defined as E(adsorbate) $+ E$(clay) $- E$(clay + adsorbate) by

considering an activated PALY framework (no zeolitic H_2O) provided with the complete or halved structural water content, as specified case by case. The number of structural water molecules before and after methyl red adsorption was considered constant.

Validation of the BEs computed with molecular mechanics simulations for zeolitic and structural water molecules in the PALY tunnels was granted by comparison with: i) experimentally obtained values for zeolitic H_2O in a similar composite system (palygorskite + indigo adduct: INDIGO@PALY hereafter); ii) BEs obtained with quantum mechanical methods for the removal of the first structural H_2O molecule (H_2O/Mg from 2 to 1 reaction) in cluster models of the PALY structure.

With this aim, an INDIGO@PALY model with 68 zeolitic water molecules in a $2a$ x b x $5c$ supercell (H_2O/Mg ratio of 3.7) was considered and optimized at the same level adopted for the METHYLRED@PALY models. The calculated BE for zeolitic H_2O (57.8 kJ/mol) proved to be in excellent agreement with the experimental value of the apparent activation energy related to loss of zeolitic H_2O in thermally treated palygorskite-indigo adducts (-56.3 ± 0.5 kJ/mol).[50] This value is also quite close to that computed for zeolitic H_2O (70.4 kJ/mol) in an analogous METHYLRED@PALY model (H_2O/Mg = 3.7).

A cluster model $Mg_2Al_4Si_{32}O_{52}H_{40} \cdot (H_2O)_4$ was adopted for the H_2O/Mg = 2 coverage (see Supporting Information, figure S1), obtained by selecting a portion of the orthorhombic structure and saturating the silicon dangling bonds with H-atoms. Consequently, a $Mg_2Al_4Si_{32}O_{52}H_{40} \cdot (H_2O)_2$ cluster model (H_2O/Mg = 1) was obtained by removing one water molecule from each Mg ion from the optimized structure of $Mg_2Al_4Si_{32}O_{52}H_{40} \cdot (H_2O)_4$.

All calculations on clusters were performed with the *Gaussian 09* software package.[51] The systems were optimized by using the Becke's (1993) three-parameters hybrid exchange functional[54] supplemented with the Lee, Yang and Parr's (1988) gradient-corrected correlation functional[55] (B3-LYP). The standard Pople basis set 3-21G was adopted for all atoms.[56] To check consistency of the BEs obtained with the B3-LYP/3-21G method and take

into account the role of the dispersive forces in the interaction, a more accurate estimation of the binding energy was also obtained by performing single point calculations at the B97D/TZVP[57,58] level. In these calculations, tight thresholds were set for the self consistent field (SCF) procedure.

Geometry optimization was carried out using the Berny optimization algorithm with analytical gradient. The thresholds were set to 0.000015 and 0.000010 a.u. for the maximum and the rms forces respectively, and 0.000060 and 0.000040 a.u. for the maximum and rms atomic displacements respectively. Accordingly, a (99,590) pruned grid was used for the B3-LYP calculations. As the importance of allowing free relaxation of the framework was demonstrated in previous theoretical studies,[59,60] no symmetry or geometrical constraints were imposed in the clusters (C_1 symmetry). Basis set superposition error (BSSE) was evaluated following the *a posteriori* method proposed by Boys and Bernardi (1970) as implemented in *Gaussian 09*.[61] From the computed binding energies (BE), the BSSE corrected binding energies (BE^c) are obtained as $BE^c = BE - BSSE$.

The optimized structures of the $Mg_2Al_4Si_{32}O_{52}H_{40} \bullet (H_2O)_4$ and $Mg_2Al_4Si_{32}O_{52}H_{40} \bullet (H_2O)_2$ clusters are reported in the Supporting Information (Figure S1). As it is evident by comparing the structures of $Mg_2Al_4Si_{32}O_{52}H_{40} \bullet (H_2O)_4$ before and after optimization, the system undergoes a strong geometry deformation. An even higher structural deformation is observed after the removal of one water molecule from each Mg ion. The deformation energy (DE) for the clay structure in this case is 223 kJ/mol. BE^c of a single structural water molecule is estimated as 30.9 kJ/mol at the B3-LYP/3-21G level and 32.6 kJ/mol at the B97D/TZVP one. Basic agreement between these values supports reliability of the results obtained with the B3-LYP/3-21G method and is an indicator of the negligible influence of dispersive forces to the interaction. If the deformation energy of the palygorskite structure is taken into account, the BE^c per water molecule [($BE_{tot}^c + DE$)/2] increases to 142.4 kJ/mol,

which is in good agreement with the value computed by means of the adopted forcefield (133.7 kJ/mol; see Table 3, section 4.2).

For these reasons, the simulated BEs of structural water for the different levels of dehydration of the composites were reported in the following because they are expected to correctly describe, at least qualitatively, the energetics of the multi-step dehydration process. Furthermore, the present approach correctly simulated the indigo@sepiolite and indigo@palygorskyte structures if compared with both experimental[42,47-49] and computational[62,63] results. The optimized structures for METHYLRED@PALY were therefore used as models to graphically guide the discussion of the experimental results.

A thermogravimetric (TG) instrument from Perkin-Elmer (Waltham, MA, USA) connected with a time-resolved FTIR and GC-MS was used to analyze the weight loss of both pristine and dye-conjugated PALY and the composition of the moieties simultaneously released from the heated samples. For the TGA analysis, the ultra-microbalance Pyris 1 from Perkin-Elmer, sensitivity 0.1 µg, was operated under a dynamic N_2 or O_2 atmosphere (30 cm^3 min^{-1}) at a heating rate of 20 °C min^{-1} in the room temperature to 1000°C interval. A relatively large sample amount (ca. 15 mg) was heated in every run to optimize the released amount of gases. Fourier transform infrared (FTIR) analysis of the gas was carried out with a Spectrum 100 (Perkin-Elmer) spectrometer equipped with a 10 cm thermostatized gas cell over a wavenumber region of 600-4000 cm^{-1}. Time/temperature-resolved infrared profile of the evolved gases were obtained by integrating the region of interest (ROI) for each molecular species investigated. In the GC-MS analysis, the desorbed moieties were in-line conducted via a pressurized transfer line (Redshift, SrL – Vicenza, Italy) heated at 300°C to a Clarus 500S gas chromatograph (Perkin-Elmer) with an integrated mass spectrometer as detector (Clarus 560S, Perkin Elmer). At a given time/temperature, ca. 100 µL of desorbed gas were injected into the GC system and a run automatically performed. The GC was operated with a standard nonpolar fused silica capillary column (DB5 MS) coated with a 5% diphenyl-

dimethylpolysiloxane stationary phase. Total ion count (TIC) chromatograms were reported as well as some detailed mass spectra of specific chromatographic peaks.

3. Results

3.1 Synchrotron-XRPD patterns

The use of synchrotron facility to collect diffraction data was dictated by the basic invariance of the XRPD patterns collected on pure PALY and on METHYLRED@PALY with conventional instruments, which is typical for these systems.[33] S-XRPD patterns of PALY and METHYLRED@PALY after background manipulation and subtraction are reported in Figure 2.
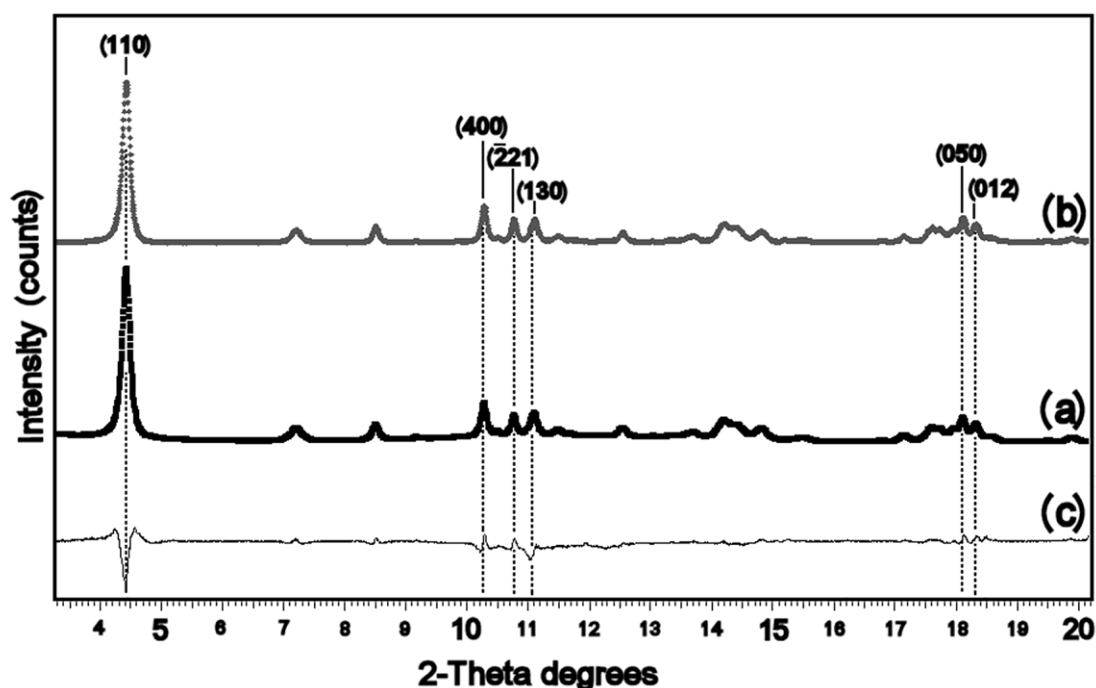
Figure 2. Comparison of normalized synchrotron XRPD patterns related to PALY (a) and METHYLRED@PALY (b). The background was manually interpolated and subtracted in both profiles. The related difference (multiplied by a factor of 2) shows subtle intensity variations which account for methyl red sorption in the host framework (c).

The analysis of the diffraction patterns was essentially aimed to: i) sharply quantify the mutual amounts of the monoclinic and orthorhombic polymorphs in the hosting framework

(PALY) and ii) estimate any manifest variation in the diffraction patterns after fixation of methyl red in the inorganic host (METHYLRED@PALY). The quantification of the relative amounts of the two polymorphs is important as monoclinic and orthorhombic PALY are known to possibly show different zeolitic water contents as well as peculiar behaviors with the incorporated guest molecules.[39] To achieve such a goal a model-constrained least-squares refinement was performed by varying only the phase scale, cell parameters and phase fractions (structural models taken from Post and Heaney[9] and Giustetto and Chiari[39] for monoclinic and orthorhombic PALY respectively). A full-profile fitting refinement of the structure of these hybrid materials with the Rietveld method, complete with atomic fractional coordinates, is not trivial due to their intrinsic complexity and to the poor scattering factor of the incorporated molecules – often present in very low amounts.[43,47,48] The contextual adoption of a multi-technical approach becomes therefore mandatory in order to possibly support these experimental data, not only by means of computational methods but also with supplementary innovative techniques (such as the ones adopted here). The performed refinement procedure showed the monoclinic fraction to be predominant (ca. 62 vs. 38%) and that no major distortion affects the clay unit cell after methyl red sorption, the detected fluctuations on a, b and c being restricted within 0.01-0.02 Å (Table 1).

	PALY		METHYLRED@PALY	
	Monoclinic	Orthorhombic	Monoclinic	Orthorhombic
Space group	*C2/m*	*Pbmn*	*C2/m*	*Pbmn*
a (Å)	13.317(5)	12.766(7)	13.297(6)	12.785(7)
b "	17.848(7)	17.852(8)	17.836(8)	17.839(9)
c "	5.247(2)	5.247(3)	5.247(2)	5.240(3)
β (°)	107.18(3)	=	107.21(2)	=
V (Å^3)	1191.5(6)	1195.6(9)	1188(1)	1195(1)
wt frac. (%)	62(1)	38(2)	61(2)	39(3)

Table 1. Space group, cell parameters and weight fractions for palygorskite and the methyl red (2 wt%) + palygorskite hybrid material (METHYLRED@PALY).

Subtle intensity differences affect some selected reflections, due to the structure factor contribution generated by the addition of the dye atoms to the host structure. The most

significant intensity variation affects the strong, low-angle (110) peak ($2\theta \cong 4.41°$; $d_{110} \cong$ 10.46 Å) which is known to be related to the channel contents.[64] This intensity fluctuation is a strong indicator of methyl red incorporation within the host channels, being associated to an increased electronic density in the pores due to the partial substitution of zeolitic H_2O with the dye in METHYLRED@PALY. Such a behavior was in fact reported in literature for similar hybrid materials.[47,65,66] Weaker intensity variations also affect the (400), (-211) and (130) peaks at $2\theta \cong 10.27°$ ($d_{400} \cong 4.47$ Å), $10.75°$ ($d_{-211} \cong 4.27$ Å) and $11.09°$ ($d_{130} \cong$ 4.14 Å), respectively. Even slighter fluctuations, presumably related to finer structural details, involve the (050) and (012) reflections at $2\theta \cong 18.10°$ ($d_{050} = 2.54$ Å) and $18.31°$ ($d_{012} = 2.50$ Å).

3.2 TGA-FTIR and GC-MS analyses

An indication about the thermal stability of METHYLRED@PALY and on the evolution with temperature rise of the stabilizing host/guest interactions was obtained by using a tandem system constituted by a thermogravimetric analyzer (TGA) whose exhaust gases were analyzed by a time-resolved FTIR and a GC-MS spectrometers. Such an apparatus allowed the sharp identification of the desorbed species responsible for the weight losses in PALY and METHYLRED@PALY respectively, and to identify those changes in the desorption temperature for zeolitic and structural water in both systems plus degradation and release of methyl red in the latter.

Figure 3 shows the TGA/TGA' profile (upper frame) and FTIR analysis (lower frame) of the thermal evolution of PALY (A) and METHYLRED@PALY (B) in the RT-800 °C range. All measured weight losses (evidenced by derivative minima, dotted line; upper frame), when directly compared to the corresponding infrared optical thermogram (obtained by

integrating the FTIR spectrum of the evolved gas in the H_2O vapor stretching region, 4000-3430 cm^{-1} in the lower frame), show an almost perfect superposition.
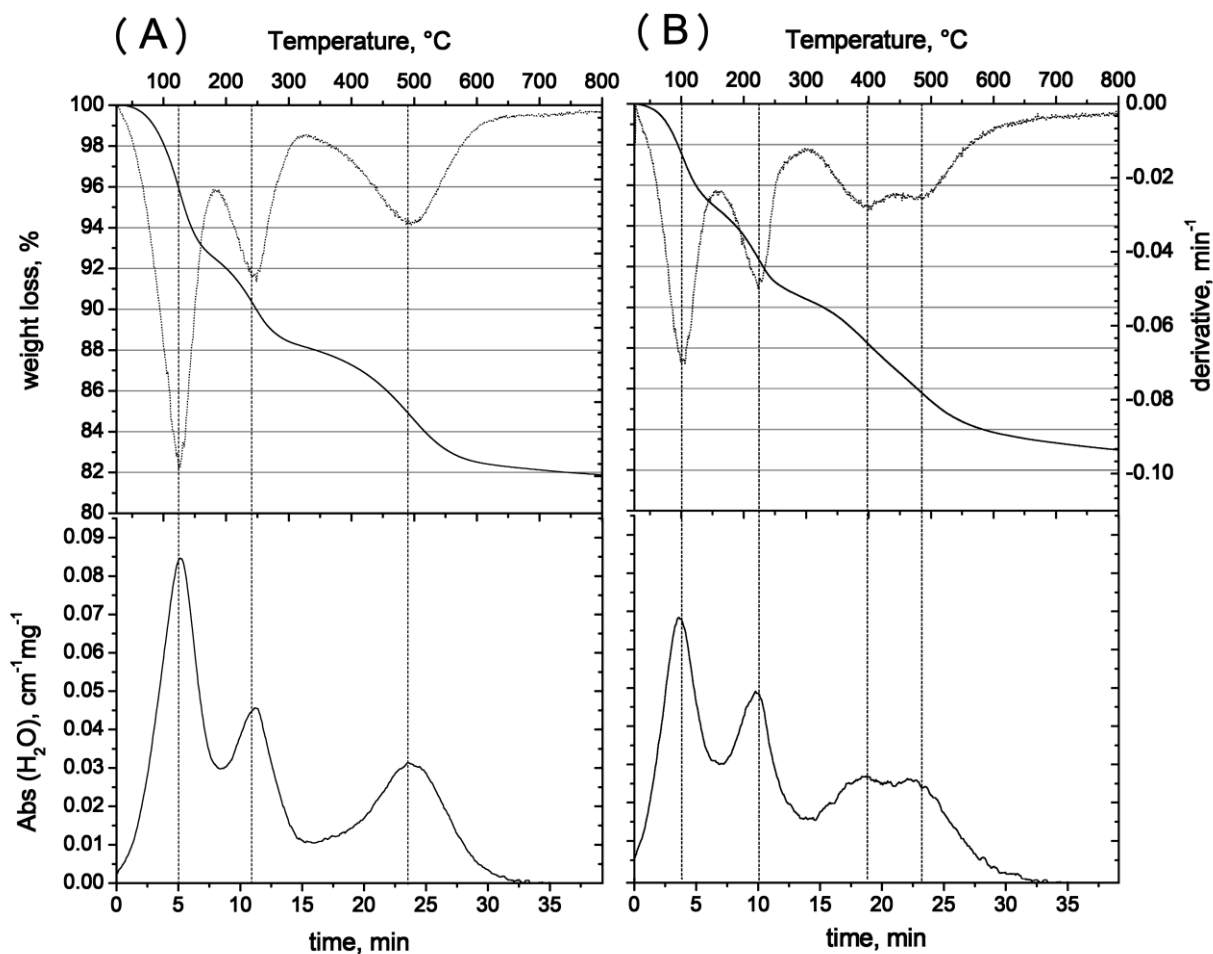
Figure 3. TGA weight loss % (full line) and derivative (dotted line) curves (upper panel) and infrared optical thermogram of H_2O evolved (lower panel, integrated frequency in the range 4000-3430 cm^{-1}) for PALY (A) and METHYLRED@PALY (B) under N_2 flow (TGA heating ramp = 20 °C/min, N_2 flow rate = 30 ml/min).

In particular, three separate weight losses can be distinguished in the heating ramp of PALY (Figure 3.A) associated to desorption/condensation of water/hydroxyls contained in the clay framework (zeolitic H_2O, structural H_2O and framework OH), in agreement with previous evidences.[9,39] In particular: i) in the RT – 150°C range, desorption of both physisorbed superficial water and zeolitic H_2O from the inner tunnels; ii) in the 200-250 °C range, release of half of structural H_2O, with consequent formation of a coordination vacancy in octahedral Mg occupying the *M3* site; iii) in the 300-600 °C range (peak at $\cong$ 485°), release

of the residual Mg-coordinated water, with phase transition to structural H_2O-deprived PALY. The recorded TGA event expands over a temperature range wider than that reported elsewhere,[9] presumably due to the different experimental setup. Loss of structural H_2O is complete well before condensation of the framework OH groups (> 650 °C), which is known to cause transformation to clinoenstatite and/or an amorphous phase.[10]

By comparing the TGA-FTIR patterns of PALY (Figure 3.A) and METHYLRED@PALY (Figure 3.B), significant variations can be noticed. It is therefore obvious that presence of methyl red in the host channels strongly affects the whole dehydration-rehydration cycle of the hybrid material, similarly to what reported in literature for analogous composites.[38,67-69] The TGA-FTIR pattern of METHYLRED@PALY (Figure 3.B), in fact, exhibits four resolved weight losses. The first two are related to release of water (as confirmed by the corresponding infrared optical thermogram – lower frame) and basically match those of PALY. However some subtle differences can be noticed. The first event (loss of superficial and zeolitic H_2O) occurs at a slightly lower temperature (100°C) in METHYLRED@PALY than in PALY (120°C); in addition, a minor weight loss is observed (5% in the composite vs. 8% in the pristine clay). The second event, associated with the desorption of the first half of structural H_2O, begins at a slightly lower T in the composite material ($\cong$ 225°C) than in the pristine clay ($\cong$ 245°C). For what concerns the desorption of the second half of structural H_2O, incorporation of the dye causes a shift in the desorption temperature but also the separation of the related signal in two separate peaks, occurring at approximately 400 and 480°C (Figure 3.B). The related infrared thermogram confirms that these two peaks are related mostly to the desorption of residual structural H_2O.

To evaluate the decomposition temperature of methyl red molecules encapsulated in the host tunnels, the TG-FTIR analysis was performed in an oxidizing atmosphere (O_2 at 30 ml/min) by monitoring the CO_2 production. Evolution of CO_2 resulting from oxidation of methyl red

shows a single event in the 350-650 °C range, with a maximum weight-loss velocity and CO_2 IR absorption at $\cong$ 500-510 °C (see Supporting Information; Figure S2).
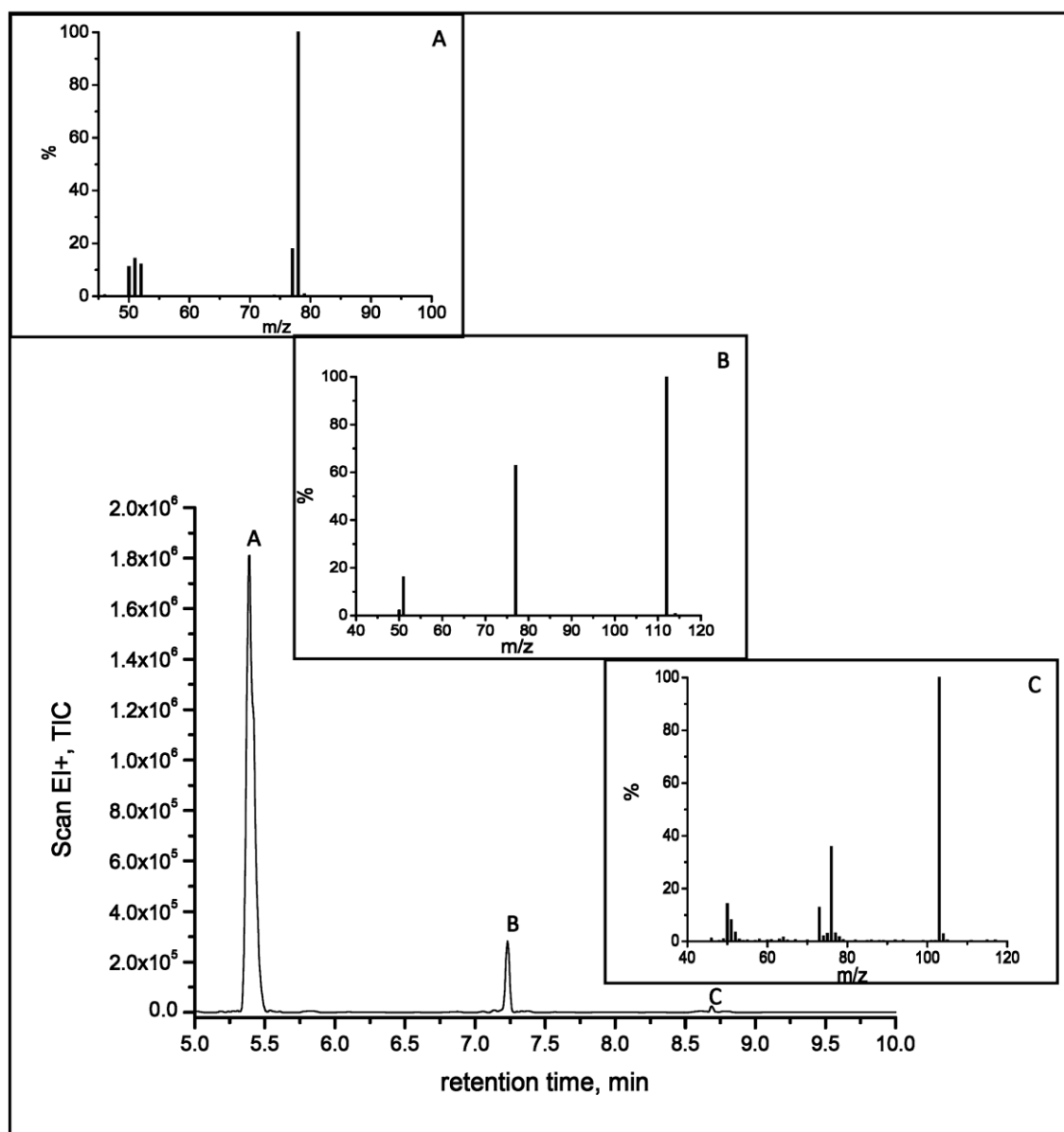
Figure 4. Gas chromatogram of the gases evolved from METHYLRED@PALY during TGA analysis at $T \cong$ 500°C under N_2 flow. In the insets (A; B; C), MS spectra related to the GC peaks are indicated.

The thermal decomposition of the clay-incorporated methyl red was measured by analyzing the TGA gas in non-oxidative conditions (N_2) injected in the GC-MS system at $T \cong$ 500 °C (maximum CO_2 flow). The corresponding chromatogram (Figure 4) shows two well resolved peaks at retention time 5.4 and 7.25 min. Analysis of the average mass spectra calculated at the peak middle height identified the two organic fragments as benzene and

chlorobenzene respectively (Figure 4, insets A and B). Traces of a third organic compound, whose mass spectrum is compatible with a N-functionalized aromatic ring, occur at a higher retention time (about 8.7 min – Figure 4, inset C). All three organic moieties are decomposition fragments of the methyl red molecule. To further elucidate the site-specific role played by the guest dye within the host tunnels, a further thermal analysis was performed on a methyl red/PALY mechanical mixture, not previously submitted to heating. In such a mixture no preliminary incorporation of methyl red in the host pores occurred, as lack of heating during synthesis prevents zeolitic H_2O desorption thus hindering dye diffusion and bonding. The weight loss, the derivative curve, and the FTIR optical thermogram of water vapor show an almost perfect superposition with data collected on PALY (see Supporting Information; Figure S3); no appreciable match with the four-minima TGA derivative curve of METHYLRED@PALY is observed. This indicates that all differences observed in the TG curves between PALY and METHYLRED@PALY – and in particular the splitting of the signal at 490°C observed only for the latter – are governed by incorporation of methyl red in the host channels and not related to any unspecific adsorption process.

3.3 Computational modeling

Molecular mechanics simulations were adopted in order to improve the understanding, from an atomistic point of view, of the nature of the host/guest interactions in METHYLRED@PALY and their evolution during heating.

The initial structures for the two polymorphs of PALY (monoclinic and orthorhombic) were based on the models used for least-squares methods.[9,39] In both cases the Mg/Al ratio was set to 1, with Mg atoms occupying the edge *M3* site (i.e. bound to structural H_2O).[70-75] Arbitrariness in the Mg/Al substitution is tolerated as the octahedral sheet occupancy is known to have negligible influences on the model geometry.[42] All calculations were

performed on a $2a$ x b x $5c$ supercell model [crystal chemical formula:

$Mg_{40}Al_{44}Si_{156}O_{400}(OH)_{40}(H_2O)_{80}$]. Four different water loadings were considered, in order to

reproduce the different ones reported in the TGA-FTIR profile: i) fully hydrated system,

where in addition to structural water, the maximum content of zeolitic water was considered

(80 molecules for both PALY and METHYLRED@PALY models, i.e. $H_2O/Mg > 2$);[5] ii)

activated system, where only structural water is present in the channels (zeolitic water

already desorbed), corresponding to the conditions reached during the pigment synthesis

(140°C in air; $H_2O/Mg = 2$); iii) half dehydrated system, where only half of the structural

water is still present in the channels ($300°C < T < 400°C$ in the experimental setup; H_2O/Mg

$= 1$); iv) fully dehydrated system, where no water molecules (no zeolitic nor structural) are

present ($H_2O/Mg = 0$). These models will be indicated hereafter using the following

acronyms: $4H_2O$, $2H_2O$, $1H_2O$ and $0H_2O$.

The excellent agreement between the experimental and calculated cell parameters for PALY

is evident by comparing those data reported in Table 2: the larger deviation consists in an

underestimation of only 3.5% for the a cell parameter, recorded in both polymorphs.

The electrostatic potential (ESP) map of a PALY channel (without zeolitic H_2O) is shown in

Figure 5: positive and negative values are reported as blue and red areas, respectively. It is

evident as strong positive values are present around the hydrogen atoms of structural H_2O,

whereas those regions surrounding the basal oxygens of the T sheet are basically apolar or

with sensibly lower ESPs.[42,48,49] In order to predict the interaction of methyl red in the

PALY channels, the ESP map for the dye molecule was also computed (Figure 5.c). The

carboxylic group evidenced a slightly negative ESP (in red: -0.06 a.u.), whereas both

methyl groups were surrounded by equivalent but opposite ESP values (in blue: $+0.06$ a.u.).

Basing on such premises, it is then expected that the grafting of the dye in the PALY

channels should involve the guest carboxylic group and the host hydrogen atoms of

structural water.

| | Monoclinic PALY | | | Orthorhombic PALY | | |
| | PALY_4H$_2$O | | PALY_2H$_2$O | PALY_4H$_2$O | | PALY_2H$_2$O |
	Exp.[9]	Calc.	Calc.	Exp.[39]	Calc.	Calc.
2a	26.572	25.736	25.610	25.344	24.427	24.079
B	17.848	18.251	18.250	17.875	18.265	18.271
5c	26.210	26.613	26.753	26.180	26.628	26.701
α	90.00	90.13	90.00	90.00	89.72	90.00
β	107.56	108.24	109.42	90.00	90.14	90.00
γ	90.00	90.02	90.00	90.00	89.98	90.00

Table 2. The 2a x b x 5c supercell parameters for PALY. Cell parameters are expressed in Å, angles in degrees.
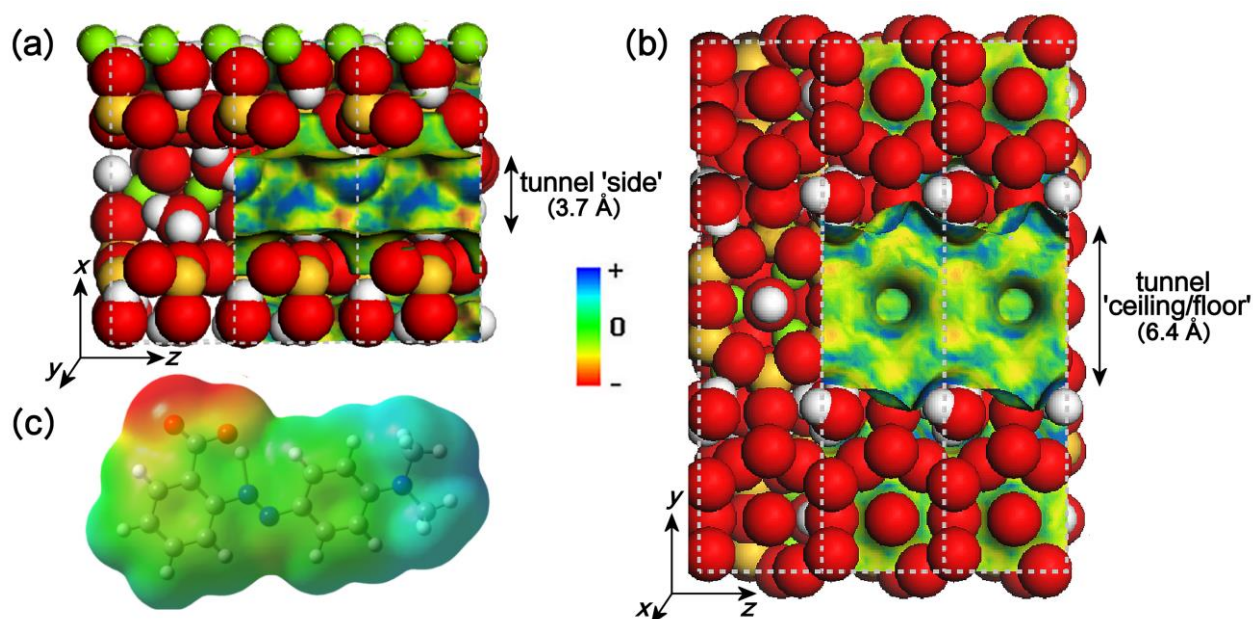
Figure 5. Electrostatic potential map of a palygorskite tunnel observed along the [010] (a) and [100] direction (b); electrostatic potential map of methyl red molecule in trans-form (c) on the 0.0004 a.u. isosurface of the electron density, as obtained from single point at the CAM-B3LYP/TZVp level. The ESP is reported in a rainbow scale; the red and blue regions correspond to ± 0.25 a.u. and 0.06 a.u. for palygorskite and methyl red respectively.

The recurrent analogies between Maya Blue and METHYLRED@PALY suggest that different topological isomers of the guest dye may simultaneously exist in the composite tunnels, consistently with its polyfunctional hybrid nature.[23-25] Previous flash photolysis and spectral studies in solution show existence of at least four conformers for methyl red in equilibrium: (i) cis, (ii) trans and (iii) (iv) two different quinoid zwitterions.[76] The cis form of methyl red, however, cannot diffuse into the tunnels because sterically hindered; absence of such a conformer in METHYLRED@PALY besides, was unequivocally confirmed by

UV-vis spectroscopy.[33] Due to this, the cis forms of the dye was excluded from the performed calculations. Incorporation in the PALY tunnels is known, on the other hand, to trigger partial transformation of methyl red from the trans to zwitterionic forms.[33,34] These zwitterions are open shell systems, both similar to the trans conformer and reputed to be mostly responsible for absorption at room temperature.[77,78] Despite this, however, because of the approximation of the molecular mechanics methods here adopted, any optimization keeping into account the zwitterionic geometries ended in the dye molecule turning back to the corresponding trans conformer. Only one out of the four different conformers – namely the trans form of methyl red – was therefore used in the performed optimizations; such a constraint, however, is not expected to undermine the obtained outcomes as this conformer represents the most reasonable approximation for the zwitterionic tautomers useable in these calculations. This limitation is further smoothed by the fact that although zwitterions apparently represent the most abundant forms at room T, the situation evolves in favour of the trans conformer once the temperature is raised (see Section 4.2).

Appearance of fair amounts of chlorobenzene in the ejected moieties deriving from fragmentation of the decomposed dye molecules at higher temperatures ($> 500°C$ – see Section 3.2), besides, brings to further considerations. The synthesis procedure of METHYLRED@PALY requires the mechanical mixture of palygorskite plus methyl red to be soaked in HCl before heating (see Section 2.1). This HCl treatment possibly causes some methyl red molecules to switch to their red protonated form,[78-80] whose positive charge is likely to be saturated by the associated chloride counterions. Subsequent heating causes this subordinated fraction of cationic methyl red molecules coupled to Cl^- anions to undergo encapsulation and bonding within the host pores, thus playing – together with the other predominant methyl red species (i.e zwitterions and trans-form) – an active role in establishing host/guest interactions with the clay framework. The protonated methyl red was therefore considered in an additional set of molecular mechanics calculations. This cationic

form of the dye was counterbalanced by a chloride anion positioned close to the peripheral

methyl groups, where the maximum positive potential region is located as suggested by the

related ESP map (see Supporting Information; Figure S4).

The METHYLRED@PALY models were obtained by adding one methyl red molecule (in

trans- or cationic form) per PALY supercell, in agreement with the experimental loading (2

wt%). Different starting geometries and alternative orientation for the different dye forms in

the clay channels were considered. The optimized results in the following always refer to the

minimum energy configuration (whose structure is reported in Figures 6, 8 and Supporting

Information; Figure S5).

The optimized disposition for the trans-form of methyl red encapsulated in an orthorhombic,

activated hosting framework (no zeolitic H_2O; METHYLRED@PALY_2H_2O) is presented

in Figure 6.a (view along [001]) and 6.b (along [100]); analogous results (not shown) were

obtained for the monoclinic polymorph. The dye molecule is juxtaposed in the centre of the

tunnel, its longer axis parallel to the z direction and approximately lying on the (100) crystal

plane. This disposition is favored on steric consideration and consistent with that of indigo

in freshly synthesized Maya Blue analogues (indigo: 4.8 x 12.3 Å; methyl red: 6.1 x 13.9 Å,

nucleus-nucleus distances).[42,48] Such an arrangement maximizes the dispersive interaction

between the guest dye and the 'sides' of the hosting matrix tunnel, causing the negative ESP

of the O=C–OH group to allow acceptance of multiple H-bonds. As expected from ESP

maps in fact, H-bonding can be identified between the structural H_2O and methyl red

COOH. The distribution of these H-bonds, however, differs in the two polymorphs: two

H_2O molecules act as donors in the monoclinic whereas three are involved in the

orthorhombic one. Direct interaction of the dye with the Al-OH groups located in the middle

of the TOT ribbons is forbidden, because sheltered by the six-membered SiO_4 rings.

Exposure to the air (and environmental moisture) of the material after synthesis was then

simulated through the addition of zeolitic water (METHYLRED@PALY_4H_2O model).

Accordingly to the experimental observations, such a trial showed that zeolitic H_2O (Figure

6.c) cannot displace the dye in the trans form nor affect the stabilizing H-bond interactions.

As far as the protonated form of methyl red is concerned, its behavior in the

METHYLRED@PALY_2H$_2$O model does not significantly differ from that of the

prevailing trans molecule. In particular, the dye is still juxtaposed in the clay tunnel and lies

flat on the (100) plane. H-bonds are formed between the COOH group of cationic methyl

red and the structural H_2O, following the same distribution observed above: two H-bonds

form in the monoclinic polymorph whereas three are observed in the orthorhombic one (see

Supporting Information; Figure S5). In both cases, the chloride anion is located close to the

H atoms of structural H_2O.
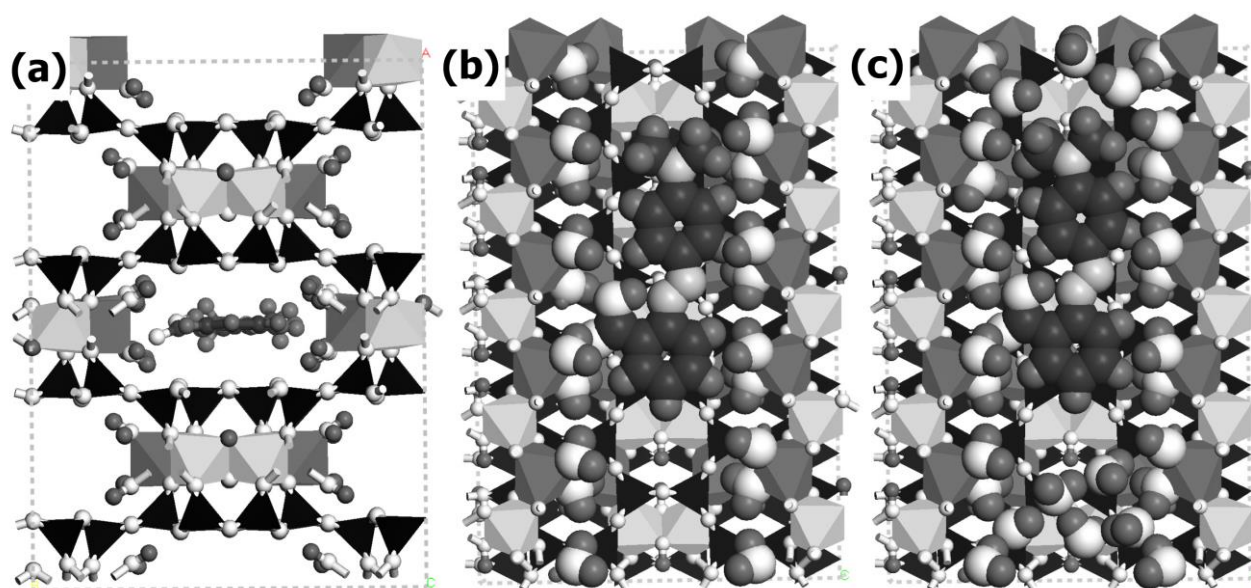
Figure 6. Optimized structure for METHYLRED@PALY_2H$_2$O (orthorhombic polymorph), as obtained by minimization with the augmented consistent-valence forcefield; view along the [001] (a) and the [100] directions (b). In (c) the optimized structure for METHYLRED@PALY_4H$_2$O(view along the [100] direction) is reported. The elements are represented in a grayscale according to the code: O (white) > N > Al > H > Mg > C > Si (black). Structural and zeolitic H_2O and methyl red (trans-form) are represented as CPK spheres. For the Si, Al and Mg atoms, the corresponding coordination polyhedrons have been used.

The evolution of the methyl red/clay interaction for T > 300°C was studied by means of the

METHYLRED@PALY_1H$_2$O and METHYLRED@PALY_0H$_2$O models (halved and total

loss of structural H_2O respectively) for both the trans- and the protonated form of methyl

red. In these models, the gradual removal of structural water is expected to cause a change in the methyl red coordination due to the availability of free coordination vacancies on the Mg^{2+} sites. In fact in METHYLRED@PALY_1H$_2$O the removal of the first half of structural H$_2$O was followed in both polymorphs by the formation of a direct bond between octahedral Mg and the carboxyl group. Moreover, when the protonated dye is concerned an additional direct interaction can form between Mg^{2+} and the chloride anions, which tend to occupy those positions left free by the structural H$_2$O loss.

An estimate of the BEs for structural water was performed for the different desorption steps limitedly to the trans-form of methyl red. These values, whose validity is confirmed by the consistency between quantum mechanical methods and molecular mechanics simulations (see Section 2.2), helped in evaluating the influence exerted by the guest dye on the peculiar dehydration of METHYLRED@PALY as evidenced by TGA data (see further discussion in Section 4.2).

4. Discussion

The collected experimental outcomes give fundamental information about the nature of the host/guest interactions and their possible evolution while heating. The dynamicity of such a process implies these interactions undergo significant variations – both in nature and strength – with progressive temperature rise, basically depending on the hydration level of the incorporating matrix. Methyl red incorporation in the tunnels significantly affects the clay dehydration process thus implying that both phenomena are correlated in a sort of mutual feedback. In order to adequately comment all encountered evidences, it is convenient to discuss separately the clay/dye interactions in the METHYLRED@PALY_2H$_2$O (full structural H$_2$O content) and in the two progressively dehydrated frameworks (METHYLRED@PALY_1H$_2$O and METHYLRED@PALY_0H$_2$O), characterized by the partial to total loss of structural

water. Finally, the degradation of the incorporated methyl red while heating and its desorption from the host is commented.

4.1 Host/guest interactions in METHYLRED@PALY_4H$_2$O and 2H$_2$O (T $\leq$ 300°C)

At room temperature the model representative of the methyl red@palygorskite system is METHYLRED@PALY_4H$_2$O, where both zeolitic H$_2$O and methyl red – in its zwitterionic, trans and/or protonated form – occupy the host channels in mutual competition, analogously to what happens in similar clay-based composites.[43,47,48,65,69] Cooling which follows the composite synthesis, in fact, causes the partly encumbered palygorskite tunnels to once again re-absorb zeolitic H$_2$O from environmental moisture, which tends to slowly but inexorably occupy those segments of the channels left free by the encapsulated dye molecules.

TGA-FTIR-GCMS results showed that further heating (at $T < 300$°C) causes one strong peak to appear in the thermal profiles for both PALY and METHYLRED@PALY, associated to the desorption of zeolitic water. However, in the latter the desorption temperature is lower than in PALY (100 instead of 120° C respectively) and the amount of released water is reduced (5% instead of 8%). Both effects can be explained as a consequence of the intervened incorporation of the dye in the host channels.[34] In fact, on one hand the decreased amount of zeolitic water could be associated to the steric hindrance due to presence of the dye in the channels. On the other hand, the lower desorption temperature can be associated to the fact that in METHYLRED@PALY the coordination vacancies surrounding the higher polarizing sites in the channels (hydrogen atoms of the structural water) are saturated by methyl red molecules. This hypothesis is supported by the calculations (see Figure 8 and Supporting Information; Figure S5) indicating that both in the METHYLRED@PALY_4H2O and in METHYLRED@PALY_2H2O, methyl red directly

interacts (in its zwitterionic, trans or protonated form) with the protons of structural water through its carboxylic group.

However, the prospected structural arrangement also suggests that the mechanism of zeolitic water desorption in PALY and METHYLRED@PALY may be completely different. In fact, the almost complete juxtaposition of methyl red and in the host pores is expected to potentially hinder, from a steric point of view, the free circulation of zeolitic H_2O and its desorption from those tunnels eventually plugged by the incorporated guest molecules. In METHYLRED@PALY, a step-by-step substitution path would therefore regulate the desorption of those zeolitic water molecules surrounding the incorporated dye, in which each H_2O molecule is 'pushed' by those queuing behind thus triggering a flowing chain which gradually bypasses the guest. An analogous mechanism, acting on both sides of the bound dye, possibly controls desorption also of structural water at higher temperatures (see Section 4.2). The constraints imposed to zeolitic H_2O are expected to obstruct $H^+(aq)$ or OH^- (aq) access to methyl red azo bond (N=N). As a result, no feasible transformation from the acid to the basic form of the dye would be allowed, thus preventing color changes and explaining the remarkable resistance of this pigment to acid or alkali attacks in aqueous solutions.[33]

4.2 Host/guest interactions in METHYLRED@PALY_1H₂O and 0H₂O (T ≥ 300°C)

To consider the evolution of the host/guest interactions at increasing temperatures (≥ 300°C), gradual loss of structural H_2O and dye decomposition must be taken into account. It is known from literature that the weight loss occurring between 200 and 250°C in PALY has to be related to departure of the first fraction of structural H_2O. Such an event originates vacancies in the coordination sphere of Mg in the *M3* site and triggers partial but progressive folding of the clay structure, with consequent reduction of the pore width and interaction of

residual H_2O with the OH groups in the middle of the six-membered SiO_4 ring[81,82] or

tetrahedral oxygens.[9] When guest dye molecules (such as indigo or methyl red) are

encapsulated in PALY or similar microporous clay minerals, however, structural folding due

to tunnel collapse is prevented;[34,65,83] despite this, the partial release of structural H_2O causes

some coordination sites on octahedral Mg to be available for formation of straight

interactions with electron donor atoms on the adsorbed dye (i.e. oxygen; Figure 7).
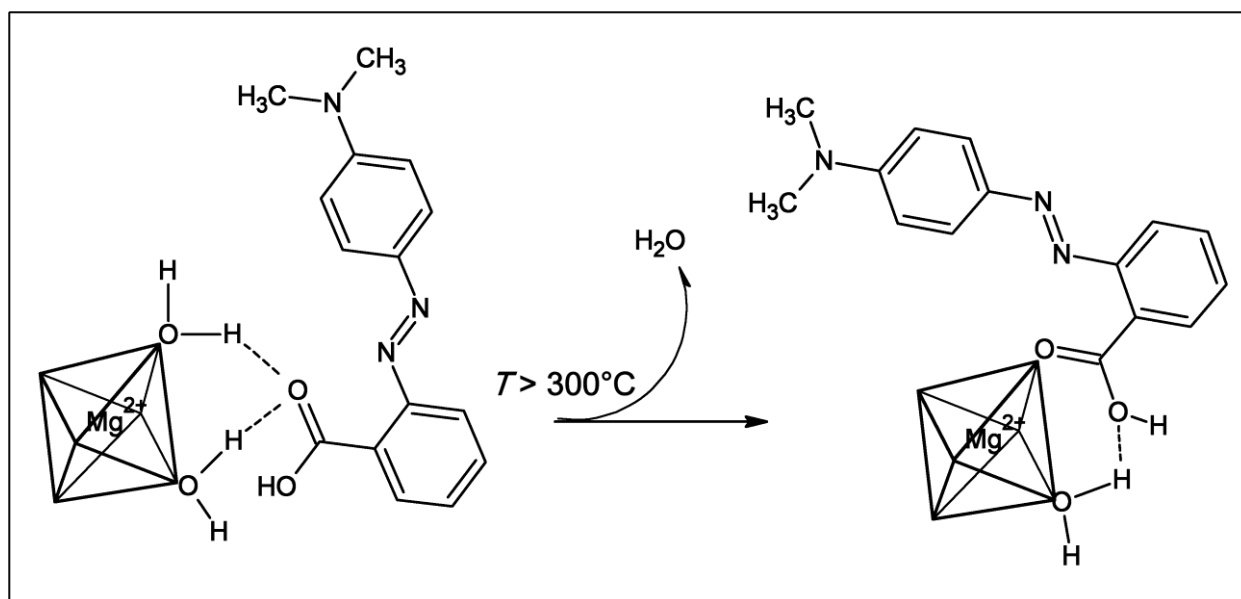
Figure 7. Methyl red-assisted elimination of the first structural H_2O molecule from octahedral Mg in the *M3* site and consequent formation of a direct Mg/COOH bond.

Molecular mechanics confirm these qualitative expectations, indicating that when a single

coordination vacancy on the octahedral Mg site is formed (only one structural H_2O molecule

bound per Mg; METHYLRED@PALY_1H2O model) direct bonding between Mg and the

methyl red COOH group occurs for both the trans- and protonated form of the dye.

Analogous bonds were previously observed in similar nano-composites submitted to severe

heating (i.e. > 280-300°C in air),[40,65,63,83-88] which tend to slowly but progressively revert to

their lower *T* configuration after cooling as a consequence of rehydration from

environmental moisture.[68,89] The same trend is likely to happen also for the studied

composite, as rehydration after cooling may undermine these high-*T* Mg/COOH interactions

and trigger re-establishment of structural H_2O-mediated H-bonds, possibly favoured from an energetic point of view (reversibility from the METHYLRED@PALY_1H_2O to METHYLRED@PALY_2H_2O model).

A direct comparison of the calorimetric results (TGA/DTG and DSC, see Supporting information, Fig. S6) shows that a lower energy amount is required to promote elimination of structural H_2O in METHYLRED@PALY with respect to INDIGO@PALY. Since the affinity to retain structural H_2O for the hosting matrix should be directly related to the strength of the H-bonding interactions formed with the incorporated dye, these experimental data suggest that the encapsulated methyl red might be less strongly bound to the PALY framework than indigo. This implies that the host/guest interactions in METHYLRED@PALY might be weaker than those in INDIGO@PALY. The higher stability of INDIGO@PALY with respect to METHYLRED@PALY can be also expected on the basis of the smaller size of indigo with respect to methyl red (4.8 x 12.3 Å and 6.1 x 13.9 Å respectively), showing the former a lower steric hindrance in the PALY tunnels. Formation of the straight methyl red COOH/octahedral Mg bonds should be expected to partially lower the desorption temperature of structural water: in METHYLRED@PALY, in fact, the breaking of the Mg/H_2O bond is partially compensated by the formation of a Mg/methyl red bond, that has no analogous counterpart in PALY. Therefore, only those structural H_2O molecules in closer proximity to the dye would be significantly affected in their stability by presence of methyl red. In the performed optimizations, four different structural H_2O molecules close to the trans-form of the dye COOH group were considered (A, B, C and D respectively in Figure 8.a). Only for the C molecule (the more perturbed one) molecular mechanics indicate that proximity of methyl red would cause a slightly anticipated removal with temperature rise. This desorption is the direct responsible for triggering the ligand-replacement process which causes the methyl red COOH group to fill the free coordination vacancy on the nearest Mg ion (Fig. 8.a') – an evolution apparently

supported by the BEs computed for the different structural H_2O molecules in each dehydration step, which confirm how the dye incorporation implies differentiation of the related energies (Table 3).

Diffuse reflectance UV-vis spectra were collected in air on the METHYLRED@PALY composite between 250 and 300°C in a previous paper,[34] showing how temperature rise causes a sensitive but selective decrease in the intensities of the absorption maxima in the visible range. In particular the main band at 540 nm, though moderately diminished in intensity, maintains its predominance while revealing a moderate – yet formerly neglected – blue-shift at 524 nm at 300°C. The maximum at 580 nm, conversely, undergoes a more evident decay presenting an analogous shift, forming at 300°C a broad shoulder at 550 nm (see Supporting Information; Fig. S7).

Persistence of the former signal, already interpreted in terms of a positive solvatochromic effect occurring during the composite synthesis,[33] suggests that stability in METHYLRED@PALY_1H$_2$O is still granted by specific host/guest interactions. The observed blue-shift, however, possibly testifies an intervened modification in these bonds nature together with their consequent weakening. The more enhanced decay of the 580 nm band, on the other hand, suggests that a gradual decrease of the zwitterions conformers in the tunnels of METHYLRED@PALY_1H$_2$O possibly occurs. This behaviour could be interpreted in terms of a diminished key-role of this particular tautomers in forming host/guest interactions. Consistently, the observed blue-shift suggests the possibility for a different tautomer – namely a modified trans-form of methyl red, yet encapsulated within the clay matrix – to be the most feasible candidate for stabilizing these high-*T* direct interactions between octahedral Mg and COOH in METHYLRED@PALY_1H$_2$O. Such an eventuality, already proposed in literature,[34] is consistent with the presumed polyfunctional organic-inorganic hybrid nature of the METHYLRED@PALY composite, characterized by different topological isomers of the guest incorporated in the host matrix and contributing to

its colour.[23-25,35,36] The recorded variations in the UV-vis spectra, in fact, imply a consequent

shift in colour of the hybrid composite at $T = 300°C$, which however pertains an intense red

hue due to the basic persistence of the maximum at 524 nm. Predominance of an altered

trans-form of methyl red in the composite at $T \geq 250°C$ is consistent with the adoption of

this particular conformer in the modelling calculations for the

METHYLRED@PALY_1H$_2$O model.
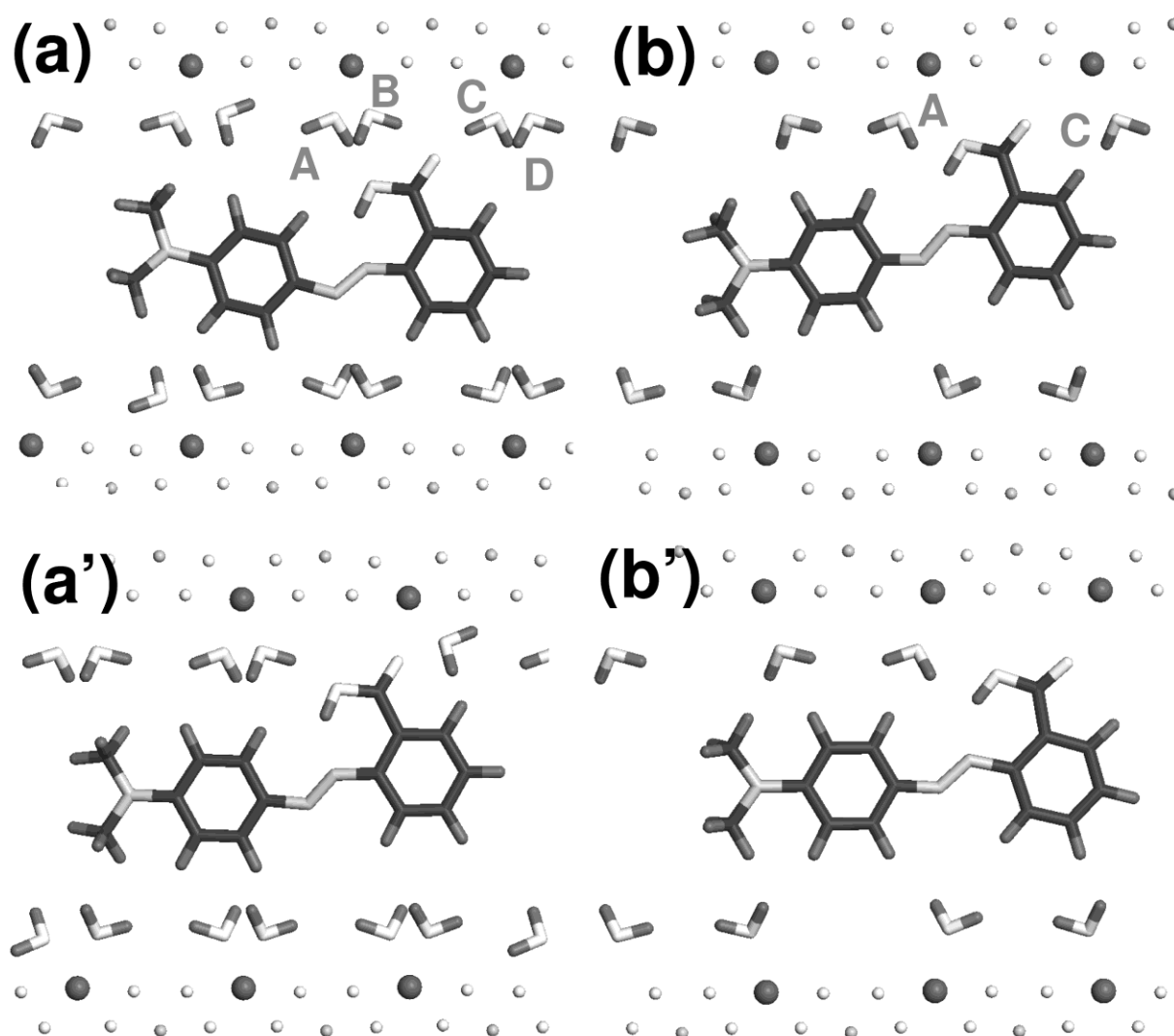
Figure 8. Optimized structures for METHYLRED@PALY (monoclinic) in the two sequential dehydration steps: (a) H$_2$O/Mg = 2 (METHYLRED@PALY_2H$_2$O), with indication of the four H$_2$O molecules (A, B, C and D) differently interacting with the COOH group of the trans-methyl red; (b) H$_2$O/Mg = 1 (METHYLRED@PALY_1H$_2$O). Removal of the H$_2$O molecule labeled C in METHYLRED@PALY_2H$_2$O and METHYLRED@PALY_1H$_2$O models brings to the (a') and (b') situations respectively, where straight interactions exist between octahedral Mg and COOH.

In the higher temperature range, a gradual decay of the dye is also expected. Thermal decomposition of the clay-conjugated methyl red starts at 350-400°C in air, when loss of resonance due to dye fragmentation causes an observable bleaching in the composite colour.[34] Despite this, the methyl red cumbersome by-products possibly still occupy the host channels in METHYLRED@PALY at T ≥ 400°C, together with yet undecomposed dye molecules in both neutral and protonated form. This situation is favored by the adopted experimental conditions (TGA-FTIR-GC-MS data collected under N_2 atmosphere), which possibly shift the dye decomposition at even higher temperatures.

Appearance of the anomalous desorption peak at 400°C in METHYLRED@PALY (Fig. 3.B) can therefore also be related to further stabilization of straight Mg/COOH interactions, analogous to those described at lower temperatures and occasionally involving also the dye fragmented moieties. Molecular mechanics showed that the release of selected structural H_2O molecules (i.e. labeled C in Figure 8.b) shortens the mutual distance between the involved reactive groups, thus increasing the chance for these direct bonds to establish and strengthen (Figure 8.b').

	PALY		METHYLRED@PALY	
Model	Monoclinic	Orthorhombic	Monoclinic	Orthorhombic
$2H_2O$	132.9	133.7	133.2, 85.0 (**D, C**) 132.9, 139.8 (**B, A**)	129.4, 80.8 (**D, C**) 130.3, 127.8 (**B, A**)
$1H_2O$	156.7	156.9	143.8 (**C**) 146.0 (**A**)	90.5 (**C**) 164.5 (**A**)

Table 3. Structural H_2O binding energies (kJ/mol) obtained for the activated ($OH_2/Mg = 2$) and half dehydrated ($OH_2/Mg = 1$) palygorskite and methyl red@palygorskite adduct with the CVFF_AUG forcefield. Please refer to Figure 8 for the legend of different H_2O molecules (A, B, C, D).

TGA data show that incorporation of methyl red in the palygorskite tunnels affects dehydration of METHYLRED@PALY with respect to pristine PALY, modifying the release of both the first and second half of structural H_2O (Figg. 3.B and 3.A respectively). In these temperature ranges the incorporated dye molecules (in their trans and/or protonated form) or their fragmented moieties act as plugs, thus obstructing the release of structural

H$_2$O trapped in the inner tunnel portions. Gradual desorption of structural H$_2$O may therefore occur only through a step-by-step substitution path involving those H$_2$O molecules bonded on both sides of the guest, in which the release of a chain link would allow the systematic advance of those queuing behind until METHYLRED@PALY_0H$_2$O is achieved. The energy necessary to switch such a process should depend on those H$_2$O molecules more strongly bound to methyl red, constituting the threshold determining the hindered step in the desorption path. When sufficient heat is administered so to allow breaking of the toughest bonds, an ordered row of H$_2$O molecules should start flowing on both sides of the dye until complete desorption. This explains why this guest-induced 'cap locking' effect can influence the whole desorption process, although the amount of H$_2$O actually interacting with the dye (and/or its fragments) is just a fraction of the total hydrous content. The modest loading of methyl red ($\leq$ 2 wt%), however, causes not every tunnel in the hybrid composite to be plugged by the dye or its decomposition by-products. Desorption of H$_2$O from these free channels should therefore not follow this step-by-step substitution path but rather the trend observed for pure PALY, thus contributing to the 480/490°C event. Such a situation may be even further complicated by the different dehydration mechanisms shown by each palygorskite polymorph (monoclinic: 62 wt%; orthorhombic: 38wt%; see Table 1), consequent to the peculiar organization of the H-bonding network which links zeolitic to structural H$_2$O.[39,70]

Further temperature rise ($\geq$ 500°C) increases methyl red fragmentation thus allowing massive departure of the guest remnants from the host tunnels (see Supporting Information, Fig. S2.B, and Section 4.3).

4.3 Release of methyl red from the METHYLRED@PALY_0H$_2$O framework (T $\geq$ 500°C)

Pure methyl red is known to decompose in air at 200-230°C, due to molecule combustion.[90] Encapsulation in the hosting matrix postpones such a phenomenon at significantly higher temperatures: an endothermic reaction in the heat flow (DSC) at 400°C was previously attributed to possible methyl red release from the host channels, consistently with the incidental bleaching of METHYLRED@PALY certified by gradual decrease until disappearance of the dye-related absorption bands in the visible spectrum.[34]

The TGA-FTIR-GC-MS data, while confirming that the endothermic reaction at 400°C is indeed related to the beginning of methyl red decomposition, prove that such an occurrence is not necessarily coincident with the desorption of the decomposed fragments from the host framework. The bulky organic moieties, in fact, do not leave at once the host framework. Their steric impediment causes them to be embedded in the PALY tunnels and bound by means of COOH-mediated interactions, thus taking an active role in the step-by-step substitution path which involves structural water desorption (see Section 4.2). Further heating implies finer fragmentation of the guest by-products, thus creating simpler moieties that can be expelled from the host framework. Coupled TGA and GC-MS data reveal traces of multiple organic fragments in the gas ejected from the composite at 500-510°C (Figure 4), when the CO_2 IR-absorption reaches its maximum (see Supporting Information, Fig. S2.B). These fragments were identified as benzene, chlorobenzene and a N-functionalized aromatic ring. The first and last molecules can undoubtedly be attributed to the intervened fragmentation of methyl red or to its decomposition by-products. Detection of the chlorinated moiety, on the other hand, is related to subordinate presence of the protonated form of the dye in the tunnels, counterbalanced by closely located chloride ions (see Sections 2.1 and 3.3). Formation of chlorobenzene is possibly due to reaction of chlorine with remnants of the incorporated dye; at $T > 450$°C the host tunnels may reasonably act as micro-reactors and possibly favor chlorination of moieties derived from methyl red fragmentation. The relatively lower amount of chlorobenzene with respect to benzene may

suggest that the protonated fraction of methyl red is subordinated to other forms (i.e. trans-isomer).

The weight loss at 480°C in METHYLRED@PALY (Fig. 3.B) can be unequivocally related to the desorption of both: i) residual structural water and ii) remnants from methyl red decomposition (though a limited loss of organic fragments at lower temperatures cannot be excluded). Their simultaneous desorption is consistent with their intimate relationship in the host tunnels, which involves METHYLRED@PALY stabilization and dehydration (see Section 4.2).

All collected evidences confirm that the thermal stability of methyl red is sensibly enhanced by the stabilizing incorporation and sheltering in the PALY pores.

5. Conclusions

The chemical reactions and molecular processes responsible for the formation of host/guest interactions in METHYLRED@PALY, a nanocomposite formed by the indissoluble union of palygorskite + methyl red, were studied in a wide temperature range using a combined multi-technique approach. The formation of this polyfunctional, inexpensive, and environmental-friendly hybrid material is achieved through the diffusion and bonding of different forms of methyl red (zwitterionic, trans and/or protonated) within the tunnels of palygorskite. The outstanding stability of METHYLRED@PALY is due to several kinds of host/guest interactions formed between the dye COOH group and the clay framework, whose evolution and/or reversibility depend on the applied heating conditions. Incorporation of the dye inside the tunnels prevents structural folding typical of PALY and modifies the host dehydration mechanism. Sheltered in the PALY pores, methyl red thermal stability is sensibly enhanced.

Acknowledgements

Supporting Information Description

Quantum mechanical calculations on palygorskite clusters; Thermal analysis and infrared optical thermogram (CO_2) for palygorskite and methyl red mechanical mixture and composite in O_2, Electrostatic potential map and molecular mechanics simulations for protonated methyl red; TGA, DTG and DSC of methyl red@palygorskite and indigo@palygorskite (*Maya Blue*) composites, Molecular mechanics results for protonated methyl red counterbalanced by chloride ion in palygorskite tunnels at different levels of hydration; UV-Vis spectra of the methyl red@palygorskite composite at increasing temperatures.

References

[1] a) Calzaferri, G.; Huber, S.; Maas, H.; Minkowski, C. Photon-Harvesting Host-Guest Antenna Materials. *Angew. Chem.* **2003**, *42*, 3860-3888; *Angew. Chem. Int. Ed. Engl.* 2003, *42*, 3732-3758; b) Brühwiler, D.; Calzaferri, G.; Torres, T.; Ramm, J.H.; Gartmann, N.; Dieu, L.Q.; Lòpez-Duarte, I.; Martìnez-Dìaz, M.V. Nanochannels for supramolecular organization of luminescent guests. J. Mater. Chem. **2009**, *19*, 8040-8067; c) Holmes, R. J.; Forrest, S. R.; Tung, Y.J.; Kwong, R. C.; Brown, J.J.; Garon, S.; Thompson, M. E. Blue organic electrophosphorescence using exothermic host-guest energy transfer. *Appl. Physics Letters* **2003**, *82*, 2422-2424.

[2] a) Salavati-Niasari, M.; Mohandes, F. Advances in Diverse Industrial Applications of Nanocomposites. Boreddy Reddy (Ed.), Intech Publ., 2011, pp. 313-352; b) Qing-Zhou, Z.; Shilun, Q.; Feng-Shou, X.; Zong-Tao, Z.; Chang-Lu, S.; Yu, H. Preparation, characterization and optical properties of the host-guest nanocomposite material zeolite-silver iodide. *Materials Research Bulletin* **2000**, *35*, 59-73; c) Gomes, R.; Albuquerque, R.Q.; Pina, F.; Parola, A.J.; De Cola, L. Supramolecular host-guest flavylium-loaded zeolite L hybrid materials: network of reactions of encapsulated 7,4prime-dihydroxyflavylium. *Photochemical and Photobiological Sciences* **2010**, *9*, 991-995; c) Easwaramoorthi, S.; Ananthanarayanan, K.; Sreedhar, B.; Natarajan, P. X-ray photoelectron spectroscopic investigation of phenosafranine adsorbed onto micro and mesoporous materials. *J. Chem. Sci.* **2009**, *121*, 711-718; d) Loera, S.; Ibarra, I.A.; Laguna, H.; Lima, E.; Bosch, P.; Lara, V.; Haro-Poniatowski, E. Colored sodalite and A zeolites. *Ind. Eng. Chem. Res.* **2006**, *45*, 9195-9200.

[3] a) Yan, D.; Lu, J.; Ma, J.; Qin, S.; Wei, M.; Evans, D.G.; Duan, X. Layered Host-Guest Materials with Reversible Piezochromic Luminescence. *Angew. Chem.* **2011**, *50*, 7175-7178; *Angew. Chem. Int. Ed. Engl.* **2011**, *50*, 7037-7040; b) Poznyak, S.K.; Tedim, J.; Rodrigues, L.M.; Salak, A.N.; Zheludkevich, M.L.; Dick, L.F.P.; Ferreira, M.G.S. Novel inorganic host layered double hydroxides intercalated with guest organic inhibitors for anticorrosion applications. *Applied Materials Interfaces* **2009**, *1*, 2353-2362; c) Ghannam, L.; Garay, H.; Billon, L. Sensitive colored hybrid inorganic/organic pigments based on polymer-coated microsized particles. *Macromolecules* **2008**, *41*, 7374-7382.

[4] a) Wirnsberger, G.; Fritzer, H.P.; van de Goor, G.; Pillep, B.; Behrens, P.; Popitsch, A. Spectroscopic investigations of novel host-guest compounds based on microporous SiO_2 frameworks and inorganic guest species. *Journal of Molecular Structure* **1997**, *410-411*, 123-127; b) Dybtsev, D.N.; Chun, H.; Kim, K. Rigid and Flexible: A Highly Porous Metal–Organic Framework with Unusual Guest-Dependent Dynamic Behavior. *Angew. Chem.* **2004**, *116*, 5033-5036; *Angew. Chem. Int. Ed. Engl.* **2004**, *116*, 5143-5146; c) Noro, S.; Kitagawa, S.; Kondo, M.; Kenji Seki. A New, Methane Adsorbent, Porous Coordination Polymer [{$CuSiF_6$(4,4′-bipyridine)$_2$}n]. *Angew. Chem.* **2000**, *39*, 2081-2084.

[5] a) Martìn Vivaldi, J.L; Cano Ruìz, J. Contribution to the study of sepiolite: II. Some considerations regarding the mineralogical formula. *Clays and Clay Minerals* **1956**, *4*, 173-176; b) Galan, E.; Carretero, M.I. A new approach to compositional limits for sepiolite and palygorskite. *Clays and Clay Minerals* **1999**, *47*, 399-409.

[6] Garcìa-Romero, E.; Suarez, M. On the chemical composition of sepiolite and palygorskite. *Clays and Clay Minerals* **2010**, *58*, 1-20.

[7] Chisholm, J.E. An X-ray powder-diffraction study of palygorskite. *Canadian Mineralogist* **1990**, *28*, 329-339; Powder-diffraction patterns and structural models for palygorskite. *Canadian Mineralogist* **1992**, *30*, 61-73.

[8] Drits, V.A.; Sokolova G.V. Structure of palygorskite. *Sov. Phys. Crystallogr.* **1971**, *16*, 183-185.

[9] Post, J.E; Heaney, P.J. Synchrotron powder diffraction study of the structure and dehydration behavior of palygorskite. *American Mineralogist* **2008**, *93*, 667-675.

[10] Preisinger, A. Sepiolite and related compounds: its stability and application. *Clays and Clay Minerals* **1963**, *10*, 365-371.

[11] Christ, C.L.; Hathaway, J.C.; Hostetler, P.B.; Shepard, A.O. Palygorskite: new X-ray data. *American Mineralogist* **1969**, *54*, 198-205.

[12] a) Bradley, W.F. The structural scheme of attapulgite. *American Mineralogist* **1940**, *25*, 405-410; b) Guggenheim, S.; Eggleton, R.A. Crystal Chemistry, classification and identification of modulated layer silicates. *Reviews in Mineralogy* **1988**, *19*, 675-725.

[13] Ferraris, G.; Makovicky, E.; Merlino S. *Crystallography of modular materials*; IUCR, Oxford University Press, Oxford, U.K., 2008.

[14] Bailey, S.W.; Alietti, A.; Brindley, G.W.; Formosa, M.L.L.; Jasmund, K.; Konta, J.; Mackenzie, R.C.; Nagasawa, K.; Rausell-Colom, R.A.; Zvyagin, B.B. Summary of recommendations of AIPEA nomenclature committee. *Clays and Clay Minerals* **1980**, *28*(*1*), 73-78.

[15] Chryssikos, G.D.; Gionis, V.; Kacandes, G.H.; Stathopoulou, E.T.; Suárez, M.; García-Romero, E.; Sánchez Del Río, M. Octahedral cation distribution in palygorskite. *American Mineralogist* **2009**, *94*, 200-203.

[16] a) Alvarez, A.; Santarén, J.; Esteban-Cubillo, A.; Aparicio P. *Developments in Palygorskite-Sepiolite Research*; E. Galan and A. Singer (Eds.), Elsevier, 2011, 281-297; b) Lòpez-Galindo, A.; Viseras, C.; Aguzzi, C.; Cerezo P. *Developments in Palygorskite-Sepiolite Research*; E. Galan and A. Singer (Eds.), Elsevier, 2011, 299-316.

[17] a) Alvarez-Ayuso, A.; Garcia-Sànchez, A. Palygorskite as a feasible amendment to stabilize heavy metal polluted soils. *Environ. Pollut.* **2003**, *125*, 337-344; b) Potgieter, J.H.; Potgieter-Vermaak, S.S.; Kalibantonga, P.D. Heavy metals removal from solution by palygorskite clay. *Minerals Engineering* **2006**, *19*, 463-470; c) Yong, K.; Jingxuan, W.; Zihliang, W.; Tao, S.; Chao, Y.; Zhidong, C. Heavy metals removal from solution by polyaniline/palygorskite composite. *Journal of Applied Polymer Science* **2011**, *122*, 2054-2059; d) Shirvani, M.; Shariatmadari, H.; Kalbasi, M.; Nourbaksha, F.; Najafi, B. Sorption of cadmium on palygorskite, sepiolite, and calcite: equilibria and organic ligand affected kinetics. *Colloids Surf*. A **2006**, *287*, 182-190; e) Shirvani, M.; Kalbasi, M.; Shariatmadari, H.; Nourbaksha, F.; Najafi, B. Sorption-desorption of cadmium in aqueous palygorskite, sepiolite and calcite suspensions: isotherm hysteresis. *Chemosphere* **2006**, *65*, 2178-2184.

[18] a) Xianzhong, B.; Gaoke, Z.; Yadan, G. Thermal modified palygorskite: preparation, characterization and application for cationic-dye containing wastewater purification. *Desalination and Water Treatment* **2011**, *30*, 339-347; b) Rui, D.; Yuanfa, L.; Xingguo, W.; Jianhua, H. Adsorption of sulphate ions from aqueous solution by surfactant-modified palygorskite. *Journal of Chemical and Engineering Data* **2011**, *56*, 3890-3896; c) Chang, P.H.; Li, Z.; Yu, T.L.; Munkhbayer, S.; Kuo, T.H.; Hung, Y.C.; Jean, J.S.; Lin, K.H. Sorptive removal of tetracycline from water by palygorskite. *Journal of Hazardous Materials* **2009**, *165*, 148-155; d) Yunfei, X.; Megharaj, M.; Ravendra, N. Adsorption of the herbicide 2,4-D on organo-palygorskite. *Appl. Clay Science* **2010**, *49*, 255-261; e) Hengpeng, Y.; Fanzhong, C.; Yanqing, S.; Guoying, S.; Jiamo, F. Adsorption of phosphate from aqueous solution onto modified palygorskites. *Separation and Purification Technology* **2006**, *50*, 283-290.

[19] a) Shariatmadari, H.; Mermut, A.R.; Benke, M.B. Sorption of selected cationic and neutral organic molecules on palygorskite and sepiolite. *Clays and Clay Minerals* **1999**, *47*, 44-53; b) Al-Futaisi, A.; Jamrah, A.; Al-Hanai, R. Aspects of cationic dye molecule adsorption to palygorskite. Desalination **2007**, *214*, 327-342; c) Ailian, X.; Shouyong, Z.; Yijiang, Z.; Xiaoping, L.; Pingfang, H. Adsorption of reactive dyes from aqueous solution by silylated palygorskite. *Appl. Clay Science* **2010**, *48*, 638-640; d) Akiuz, S.; Akiuz, T.; Akalin, E. Adsorption of isoniazid onto sepiolite-palygorskite group of clays: an IR study. *Spectrochim. Acta A, Mol. Biomol. Spectrosc.* **2010**, *75*, 1304-1307; e) Hao, C.; Jie, Z.; Aiguo, Z.; Yanxian, J. Removal capacity and adsorption mechanism of heat-treated palygorskite clay for methilene blue. *Chemical Engineering Journal* **2011**, *174*, 143-150.

[20] a) Reyes-Valerio, C. *De Bonampak al Templo Mayor: el Azul Maya en Mesoamerica*. Siglo XXI (Ed.), Mexico City, 1993. b) Arnold, D.E.; Bohor, B.F.; Neff, H.; Feinman, G.M.; Williams, P.R.; Dussubieux, L.; Bishop, R. The first direct evidence of pre-Columbian sources of palygorskite for Maya Blue. *Journal of Archaeological Science* **2012**, *39*, 2252-2260.

[21] Lima, E.; Guzman, A.; Vera, M.; Rivera, J.L.; Fraissard, J. Aged natural and synthetic Maya Blue-like pigments: what difference does it make? *J. Phys. Chem. C* **2012**, *116*(*7*), 4556-4563.

[22] Sànchez del Rìo, M.; Doménech, A.; Doménech-Carbò, M.T.; Vàzquez de Agredos Pascual, M.L.; Suàrez, M.; Garcìa-Romero, E. *Developments in Palygorskite-Sepiolite Research*; E. Galan and A. Singer (Eds.), Elsevier, 2011, 453-481.

[23] Doménech, A.; Doménech-Carbò, M.T.; Vàzquez de Agredos Pascual, M.L.Dehydroindigo: A New Piece into the Maya Blue Puzzle from the Voltammetry of Microparticles Approach. *J. Phys. Chem. B* **2006**, *110*, 6027-6039.

[24] Doménech, A.; Doménech-Carbò, M.T.; Vàzquez de Agredos Pascual, M.L.Indigo/dehydroindigo/palygorskite complex in Maya Blue: an electrochemical approach. *J. Phys. Chem. C* **2007**, *111*, 4585-4595.

[25] Doménech, A.; Doménech-Carbò, M.T.; Sànchez del Rìo, M.; Goberna, S.; Lima, E. Evidence of topological indigo/dehydroindigo isomers in Maya Blue-like complexes prepared from palygorskite and sepiolite. *J. Phys. Chem. C* **2009**, *113*, 12118-12131.

[26] Gettens, R.J. Maya Blue: an unsolved problem in ancient pigments. *American Antiquity* **1962**, *27*, 557-564.

[27] Van Olphen, H. Maya Blue: a clay-organic pigment? *Science* **1966**, *154*, 645-646.

[28] Kleber, R.; Masschelein-Kleiner, L.; Thissen, J. Étude et identification du "Bleu Maya". *Studies in Conservation* **1967**, *12*, 41-55.

[29] Reinen, D.; Köhl, P.; Muller, C. Colour centres in 'Maya Blue' – the incorporation of organic pigment molecules into the palygorskite lattice. *Zeitschrift für anorganische und allgemeine Chemie* **2004**, *630*, 97-103.

[30] Dejoye, C.; Martinetto, P.; Dooryhée, E.; Strobel, P.; Blanc, S.; Bordat, P.; Brown, R.; Porcher, F.; Sanchez del Rìo, M.; Anne, M. Indigo@silicalite: a new organic-inorganic hybrid pigment. *Applied Materials & Interfaces* **2010**, *8*, 2308-2316.

[31] Dejoye, C.; Martinetto, P.; Dooryhée, E.; Van Elslande, E.; Blanc, S.; Bordat, P.; Brown, R.; Porcher, F.; Anne, M. Association of indigo with zeolites for improved color stabilization. *Applied Spectroscopy* **2010**, *64*, 1131-1138.

[32] Kowalak, S.; Zywert, A. Preparation of Maya Blue analogues using natural zeolites. *Clay Minerals* **2011**, *46(2)*, 197-204.

[33] Giustetto, R.; Wahyudi, O. Sorption of red dyes on palygorskite: synthesis and stability of red/purple Mayan nanocomposites. *Microporous and Mesoporous Materials* **2011**, *142*, 221-235.

[34] Giustetto, R.; Seenivasan, K.; Pellerej, D.; Ricchiardi, G.; Bordiga, S. Spectroscopic characterization and photo-thermal resistance of a hybrid palygorskite/methyl red Mayan pigment. *Microporous and Mesoporous Materials* **2012**, *155*, 167-176.

[35] Doménech, A.; Doménech-Carbò, M.T.; Valle-Algarra, F.M.; Domine, M.E.; Osete-Cortina, L. On the dehydroindigo contribution to Maya Blue. *J. Mater. Sci.* **2013**, *48*, 7171-7183.

[36] Doménech, A.; Valle-Algarra, F.M.; Doménech-Carbò, M.T.; Domine, M.E.; Osete-Cortina, L.Gimeno-Adelantado, J.V. Redox tuning and species distribution in Maya-Blue type materials- a reassesment. *Applied Materials & Interfaces* **2013**, *5*, 8134-8145.

[37] Doménech, A.; Doménech-Carbò, M.T.; Sànchez del Rìo, M.; Vàzquez de Agredos Pascual, M.L. Comparative study of different indigo-clay Maya Blue-like systems using the voltammetry of microparticles approach. *J. Solid State Electrochem.* **2009**, *13*, 869-878.

[38] Sànchez del Rìo, M.; Boccaleri, E.; Milanesio, M.; Croce, G.; Van Beek, W.; Tsiantos, C.; Chryssikos, D.; Gionis, V.; Kacandes, G.H.; Suarez, M.; Garcia-Romero, E. A combined synchrotron powder diffraction and vibrational study of the thermal treatment of palygorskite-indigo to produce Maya Blue. *J. Mater. Sci.* **2009**, *44*, 5524-5536.

[39] Giustetto, R.; Chiari, G. Crystal structure refinement of palygorskite from neutron powder diffraction. *Eur. Journ. of Mineral.* **2004**, *16*, 521-532.

[40] Polette-Niewold, L.A.; Manciu, F.S.; Torres, B.; Alvarado Jr, M.; Chianelli, R.R. Organic/inorganic complex pigments: Ancient colors Maya Blue. *Journal Of Inorganic Biochemistry* **2007**, *101*, 1958-1973.

[41] Sànchez Del Rìo, M.; Martinetto, P.; Reyes-Valerio, C.; Dooryhée, E.; Suárez, M. Synthesis and acid resistance of Maya Blue pigment. *Archaeometry* **2006**, *48*, 115-130.

[42] Giustetto, R.; Llabres I Xamena, F.; Ricchiardi, G.; Bordiga, S.; Damin, A.; Chierotti, M.R.; Gobetto, R. Maya Blue: a computational and spectroscopic study. *J. Phys. Chem. B* **2005**, *109(41)*, 19360-19368.

[43] Giustetto, R.; Levy, D.; Chiari, G. Crystal structure refinement of Maya Blue pigment prepared with deuterated indigo, using neutron powder diffraction. *Eur. Journ. of Mineral.* **2006**, *18*, 629–640.

[44] a) Larson, A.C.; Von Dreele, R.B. General Structure Analysis System (GSAS). *Los Alamos National Laboratory Report LAUR* **1994**, 86-748; b) Toby, B. H. EXPGUI, a graphical user interface for *GSAS*. *J. Appl. Cryst.* **2001**, *34*, 210-213.

[45] Materials Studio 5.0, Discover module, Accelerys Incorporated **2009**, San Diego, CA.

[46] Dauber-Osguthorpe, P.; Roberts, V.A.; Osguthorpe, D.J.; Wolff, J.; Genest, M.; Hagler, A.T. Structure and energetic of ligand binding to proteins: Escherichia coli dihydrofolate reductase-tripethoprim, a drug receptor system. *Proteins* **1988**, *4*(*1*), 31-47.

[47] Chiari, G.; Giustetto, R.; Ricchiardi, G. Crystal structure refinements of palygorskite and Maya blue from molecular modeling and powder synchrotron diffraction. *Eur. J. Mineral.* **2003**, *15*, 21-33.

[48] Giustetto, R.; Levy, D.; Wahyudi, O.; Ricchiardi, G.; Vitillo, J.G. Crystal structure refinement of a sepiolite/indigo Maya Blue pigment using molecular modeling and synchrotron diffraction. *Eur. J. Mineral.* **2011**, *23*, 449-466.

[49] Chiari, G.; Giustetto, R.; Druzik, J.; Doehne, E.; Ricchiardi, G. Pre-columbian nanotechnology: reconciling the mysteries of the Maya Blue pigment. *Appl. Phys. A* **2008**, *90*(*1*), 3-7.

[50] Doménech, A.; Doménech-Carbò, M.T.; Osete-Cortina, L.; Montoya, N. Application of solid state electrochemistry techniques to polyfunctional organic-inorganic hybrid materials: the Maya Blue problem. *Microporous and Mesoporous Materials* **2013**, *166*, 123-130.

[51] Frisch, M.J.; Trucks, G.W.; Schlegel, H.B.; Scuseria, G.E.; Robb, M.A.; Cheeseman, J.R.; Scalmani, G.; Barone, V.; Mennucci, B.; Petersson, G.A. et al. *Gaussian 09, Revision* A.02 2009, Gaussian, Inc.; Wallingford CT.

[52] Vogiatzis, K. D.; Mavrandonakis, A.; Klopper, W.; Froudakis, G. E. Ab initio study of the interactions between CO_2 and N-containing organic heterocycles. *ChemPhysChem* **2009**, *10*, 374-383.

[53] Vitillo, J. G.; Groppo, E.; Bordiga, S.; Chavan, S.; Ricchiardi, G.; Zecchina, A. Stability and reactivity of grafted $Cr(CO)_3$ species on MOF linkers: a computational study. *Inorg. Chem.* **2009**, *48*, 5439-5448.

[54] Becke, A. D. Density-Functional Thermochemistry. III. The Role of Exact Exchange. *J. Chem. Phys* **1993**, *98*, 5648-5652.

[55] Lee, C.; Yang, W.; Parr, R.G. Development of the Colle-Salvetti correlation-energy formula into a functional of the electron density. *Phys. Rev. B* **1988**, *37*, 785-789.

[56] a) Gordon, M.S. The isomers of silacyclopropane. *Chem. Phys. Lett.* **1980**, *76*,163–168; b) Hariharan, P.C.; Pople, J.A. The influence of polarization functions on molecular orbital hydrogenation energies. *Theor. Chim. Acta* **1973**, *28*, 213-222; c) Hariharan, P.C.; Pople, J.A. Accuracy of AH, Equilibrium Geometries by Single Determinant Molecular Orbital Theory. *Mol. Phys.* **1974**, *27*, 209-214; d) Hehre, W.J.; Radom, L.; Schleyer, P.v.R.; Pople, J.A. Ab Initio Molecular Orbital Theory. **1986**, John Wiley & Sons, New York, 548 pp.; e) Frisch, M.J.; Pople, J.A.; Binkley, J.S. Self Consistent Molecular Orbital Methods. 25. Supplementary Functions for Gaussian Basis Sets. *J. Chem. Phys.* **1984**, *80*, 3265-3269; f) Clark, T.; Chandrasekhar, J.; Spitznagel, G.W.; Schleyer, P.v.R. Efficient diffuse function-augmented basis sets for anion calculations. III. The 3-21+G basis set for first-row elements, Li– F. *J. Comp. Chem.* **1983**, *4*, 294-301.

[57] Grimme, S. Semiempirical GGA-type density functional constructed with a long-range dispersion correction. *J. Comp. Chem.*, **2006**, *27*, 1787-1799.

[58] a) Schäfer, A.; Huber, C.; Ahlrichs, R. Fully optimized contracted gaussian basis sets of triple zeta valence quality for atoms Li to Kr. J. Chem. Phys. **1994**, *100(8)*, 5829-5835; b) Schäfer, A.; Horn, H.; Ahlrichs, R. Fully optimized contracted gaussian basis sets for atoms Li to Kr. *J. Chem. Phys.* **1994**, *97*, 2571.

[59] Uzunova, E. L.; Nikolov, G. S. DFT study of zeolite LTA structural fragments: double four-member rings of oxygen-bridged silicon and aluminum atoms. *J. Phys. Chem. A* **2000**, *104(22)*, 5302-5306.

[60] Higgins, F. M.; Watson, G. W.; Parker, S. C. Effect of relaxation on cation exchange in zeolite A using computer simulation. *J. Phys. Chem. B* **1997**, *101*, 9964-9972.

[61] Boys, S. F.; Bernardi, F. Calculations of small molecular interactions by differences of separate total energies – some procedures with reduced errors. *Mol. Phys.* **1970**, *19*, 553-566.

[62] Fois, E.; Gamba, A.; Tilocca, A. On the unusual stability of Maya Blue paint: molecular dynamics simulations. *Microporous and Mesoporous Materials* **2003**, *57*, 263-272.

[63] Tilocca, A.; Fois, E. The colour and stability of Maya Blue: TDDFT calculations. *J. Phys. Chem. C* **2009**, *113*, 8683-8687.

[64] a) Norby, P.; Poshni, F.I.; Gualtieri, A.F.; Hanson, J.C.; Grey, C.P. Cation migration in zeolites: an in situ powder diffraction and MAS NMR study of the structure of zeolite Cs(Na)-Y during dehydration. *J. Phys. Chem. B* **1998**, *102*, 839-856; b) Dalconi, M.C.; Alberti, A.; Cruciani, G. Cation migration and structural modification of Co-exchanged ferrierite upon heating: a time-resolved X-ray powder diffraction study. *J. Phys. Chem. B* **2003**, *107*, 12973-12980; c) Dalconi, M.C.; Cruciani, G.; Alberti, A.; Ciambelli, P. Over-loaded Cu-ZSM-5 upon heating treatment: a time resolved X-ray diffraction study. *Microporous and Mesoporous Materials* **2006**, *94*, 139-147; d) Cruciani, G. Zeolites upon heating: factors governing their thermal stability and structural changes. *Journal of Physics and Chemistry of Solids* **2006**, *67*, 1973-1994; e) Martucci, A.; Guzman-Castillo, M.d.L.; Di Renzo, F.; Fajula, F.; Alberti, A. Reversible channel deformation of zeolite omega during template degradation highlighted by in situ time-resolved synchrotron powder diffraction. *Microporous and Mesoporous Materials* **2007**, *104*, 257-268; f) Agostini, G.; Lamberti, C.; Palin, L.; Milanesio, M.; Danilina, N.; Xu, B.; Janousch, M.; van Bokhoven, J.A. In situ XAS and XRPD parametric Rietveld refinement to understand dealumination of Y zeolite catalyst. *J. Am. Chem. Soc*. **2010**, *132*, 667-678.

[65] Ovarlez, F.; Giulieri, S.; Chaze, A.M.; Delamare, F.; Raya, J.; Hirschinger, J. The incorporation of indigo molecules in sepiolite tunnels. *Chem. Eur. J.* **2009**, *15*, 11326-11332.

[66] Yasarawan, N.; Van Duijneveldt, J.S. Dichroism in dye-doped colloidal liquid crystals. Langmuir **2008**, *24*, 7184-7192.

[67] Giustetto, R.; Seenivasan, K.; Bonino, F.; Ricchiardi, G.; Bordiga, S.; Damin, A.; Chierotti, M.R.; Gobetto, R. Host/guest interactions in a sepiolite-based Maya Blue pigment: a spectroscopic study. *J. Phys. Chem. C* **2011**, *115*(*41*), 16764-16776.

[68] Tsiantos, C.; Tsampodimou, M.; Kacandes, G.H.; Sanchez del Rìo, M.; Gionis, V.; Chryssikos, G.D. Vibrational investigation of indigo-palygorskite association(s) in synthetic Maya blue. *Journal of Materials Science* **2012**, *47*(*7*), 3415-3428.

[69] Giustetto, R.; Wahyudi, O.; Corazzari, I.; Turci, F. Chemical stability and dehydration behavior of a sepiolite/indigo Maya Blue pigment. *Appl. Clay Science* **2011**, *52*, 41-50.

[70] Serna, C.; Van Scoyoc, G.E.; Ahlrichs, J.L. Hydroxyl groups and water in palygorskite. *American Mineralogist* **1977**, *62*, 784-792.

[71] Heller-Kallai, L.; Rozenson, I. MÖssbauer Studies of Palygorskite and Some Aspects of Palygorskite Mineralogy. *Clays and Clay Minerals* **1981**, *29*, 226-232.

[72] Corma, A.; Mifsud, A.; Sanz, E. Kinetics of the acid leaching of palygorskite: influence of the octahedral sheet composition. *Clay Minerals* **1990**, *25*, 197-205.

[73] Garcia-Romero, E.; Suàrez Barrios, M.; Bustillo Revuelta, M.A. Characteristic of a Mg-palygorskite in Miocene rocks (Madrid Basin, Spain). *Clays and Clay Minerals* **2004**, *52*, 486-494.

[74] Suàrez, M.; Garcia-Romero, E. FTIR spectroscopic study of palygorskite: influence of the composition of the octahedral sheet. *Appl. Clay Science* **2006**, *31*, 154-163.

[75] Giustetto, R.; Compagnoni, R. An unusual occurrence of palygorskite from Montestrutto, Sesia-Lanzo Zone, Internal Western Alps (Italy). *Clay Minerals* **2011**, *46*, 371-385.

[76] a) Whitten, D.G.; Wildes, P.D.; Pacifici, J.C.; Irick, G. Jr.; Solvent and substituent on the thermal isomerization of substituted azobenzenes, Flash spectroscopic study. *Journal of the American Chemical Society* **1971**, 93, 2004-2008. b) Nishimura, N.; Kosako, S.; Sueishi, Y. The thermal isomerization of azobenzenes, III. Substituent, solvent and pressure effects on the thermal isomerization of push-pull azobenzenes. *Bulletin Chemical Society of*

Japan **1984**, *67*, 1617-1625. c) Biswas, N.; Umapathy, S. Structures, vibrational frequencies and normal modes of substituted azo dyes: infrared, Raman and Density Functional calculations. *J. Phys. Chem. A* **2000**, *104(12)*, 2734–2745.

[77] Mukherjee, S.; Chandra Bera, S. Low temperature laser flash photolysis and spectral studies of Methyl Red. *J. Chem. Soc., Faraday Trans*. **1998**, *94(1)*, 67- 71.

[78] Benedict, J.B.; Cohen, D.E.; Lovell, S.; Rohl, A.L.; Kahr, B. What is syncristallization? States of the pH indicator Methyl Red in crystals of phtalic acid. *Journal of the American Chemical Society* **2006**, *128(16)*, 5548- 5559.

[79] Tawarah, K.M.; Abu-Shamleh, H.M. A spectrophotometric study of the acid-base equilibria of *o*-methyl red in aqueous solutions. *Dyes and Pigments* **1991**, *17*, 203–215.

[80] Gonzalez, C.; Touraud, E.; Spinelli, S.; Thomas, O. *UV–visible Spectrophotometry of Water and Wastewater*. O. Thomas and C. Burgess (Eds.), , 2007, 57–58.

[81] Hayashi, H.; Otsuka, R.; Imai, N.. Infrared study of sepiolite and palygorskite on heating. *American Mineralogist* **1969**, *54*, 1613-1624.

[82] Van Scoyoc, G.E.; Serna, C.J.; Ahlrichs, J.L. Structural changes in palygorskite during dehydration and dehydroxylation. *American Mineralogist* **1979**, *64*, 215–223.

[83] Giulieri, F.; Ovarlez, S.; Chaze, A.M. Indigo/sepiolite nanohybrids: stability of natural pigments inspired by Maya Blue. *International Journal of Nanotechnology* **2012**, *9*, 605-617.

[84] Manciu, F.S.; Ramirez, A.; Durrer, W.; Govani, J.; Chianelli, R.R. Spectroscopic analysis of a dye-mineral composite − a Raman and FT-IR study. *Journal Of Raman Spectroscopy* **2008**, *39*, 1257-1261.

[85] Fuentes, M.E.; Peňa, B.; Contreras, C.; Montero, A.L.; Chianelli, R.; Alvarado, M.; Olivas, R.; Rodrìguez, L.M.; Camacho, H.; Montero-Cabrera, L.A. Quantum mechanical model for Maya Blue. *Int. Journ. of Quantum Chem*. **2008**, *108(10)*, 1664-1673.

[86] Kuang, W.; Facey, G.A.; Detellier, C. Organo-mineral nanohybrids. Incorporation, coordination and structuration role of acetone molecules in the tunnels of sepiolite. *J. Mater. Chem.* **2006**, *16*, 179-185.

[87] Raya, J.; Hirschinger, J.; Ovarlez, S.; Giulieri, F.; Chaze, A.M.; Delamare, F. Insertion of indigo molecules in the sepiolite structure as evidences by [1]H-[29]Siheteronuclear correlation spectroscopy. *Phys. Chem. Chem. P*. **2010**, *12*, 14508-14514.

[88] Martìnez-Martìnez, V.; Corcòstegui, C.; Bañuelos Prieto, J.; Gartzia, L.; Salleres, S.; López Arbeloa, I.J. Distribution and orientation study of dyes intercalated into single sepiolite fibers. A confocal fluorescence microscopy approach. *J. Mater. Chem.* **2011**, *21*, 269–276.

[89] Ovarlez, S.; Giulieri, F.; Delamare, F.; Sbirrazzuoli, N.; Chaze, A.M. Indigo-sepiolite nanohybrids: temperature-dependent synthesis of two complexes and comparison with indigo-palygorskite systems. *Microporous and Mesoporous Materials* **2011**, *142*, 371-380.

[90] Tian, Y.; Wang, G.; Li, F.; Evans, D.G. Synthesis and thermo-optical stability of *o*-methyl red-intercalated Ni–Fe layered double hydroxide material. *Materials Letters* **2007**, *61*, 1662-1666.

Table of Contents (TOC) Image